Human-induced climate change increased drought severity in Horn of Africa

1. Joyce Kimutai, *Kenya Meteorological Department, Nairobi, Kenya*
2. Clair Barnes, *Grantham Institute, Imperial College London, UK*
3. Mariam Zachariah, *Grantham Institute, Imperial College, London, UK*
4. Sjoukje Philip, *Royal Netherlands Meteorological Institute (KNMI), De Bilt, The Netherlands*
5. Sarah Kew, *Royal Netherlands Meteorological Institute (KNMI), De Bilt, The Netherlands*
6. Izidine Pinto, *Royal Netherlands Meteorological Institute (KNMI), De Bilt, The Netherlands*
7. Piotr Wolski, *Climate System Analysis Group, University of Cape Town, Cape Town, South Africa*
8. Gerbrand Koren, *Copernicus Institute of Sustainable Development, Utrecht University, Utrecht, the Netherlands*
9. Gabriel Vecchi, *Department of Geosciences, Princeton University, Princeton, NJ 08544, USA, High Meadows Environmental Institute, Princeton University, Princeton, NJ 08544, USA*
10. Wenchang Yang, *Department of Geosciences, Princeton University, Princeton, NJ 08544, USA*
11. Sihan Li, *Department of Geography, University of Sheffield*
12. Maja Vahlberg, *Red Cross Red Crescent Climate Centre, The Hague, the Netherlands*
13. Roop Singh, *Red Cross Red Crescent Climate Centre, The Hague, the Netherlands*
14. Dorothy Heinrich, *Red Cross Red Crescent Climate Centre, The Hague, the Netherlands*
15. Carolina Marghidan Pereira, *Faculty of Geo-Information Science and Earth Observation (ITC), University of Twente, Enschede, the Netherlands; Red Cross Red Crescent Climate Centre, The Hague, the Netherlands*
16. Julie Arrighi, *Red Cross Red Crescent Climate Centre, The Hague, the Netherlands; Global Disaster Preparedness Center, Washington DC, USA; University of Twente, The Netherlands*
17. Lisa Thalheimer, *United Nations University, Institute for Environment and Human Security, Bonn, Germany*
18. Cheikh Kane, *Red Cross Red Crescent Climate Centre, The Hague, the Netherlands*; *Institut de Recherche pour le Développement, U01000/99AA01, Marseille, France*
19. Friederike E. L Otto, *Grantham Institute, Imperial College London, UK*

Main findings

- The Southern part of the Horn of Africa, covering parts of southern Ethiopia, southern Somalia, and eastern Kenya (see figure 1), saw below average rainfall for the short rains (October-December) in 2020, 2021 and 2022 as well as the long rains (March-May) in 2021 and 2022.
- As one of the world's most impoverished regions, the Horn of Africa is home to millions of people facing chronic food and water insecurity, malnutrition, and limited access to basic services including infrastructure, health care, education, and social welfare. The ongoing drought has turned these underlying conditions into acute food insecurity for over 4 million inhabitants.
- In order to identify whether human-induced climate change was a driver of the low rainfall, i.e the meteorological drought, we analysed rainfall over the most impacted region in the Southern

https://doi.org/10.25561/102624

Horn of Africa, covering parts of southern Ethiopia, southern Somalia, and eastern Kenya, for 24 consecutive months, from January 2021 to December 2022, as well as just the individual 2022 March-May and October-December seasons separately.

- We find that in today's climate, which has been warmed about 1.2°C by human-induced greenhouse gas emissions, the below-average rainfall in the March-May season is a 1 in 10 year event, a 1 in 5 year event in the short rains. For the entire 24-month period there is a 5% chance in every year for such an event to develop.
- Using two observation-based rainfall products we find there is a trend towards less rainfall in the long rains but not over the short rains, which show the opposite, a wettening. There is no trend when looking at the short and long rains combined over 24 months.
- The years of the drought also saw consecutive La Niña conditions. There is a high correlation between below-average short rains and La Niña, but there is no correlation with the long rains. When taking into account the effect of La Niña there is a trend towards wetter conditions in the short rains.
- To formally attribute these trends to climate change and to try to quantify its contribution to the drought, we used climate models and looked at similarly low rainfall events over the same region in the model data. We found that the models show similar results to the observations: low rainfall events like those currently observed in the long rains have become about twice as likely due to human-induced climate change, while there is no attributable change when short and long rains are combined. In the short rains, models where the effect of La Niña is taken into account show that a low rainfall season like the one observed has become less likely, making the increased rainfall in the short rains attributable to human-induced climate change.
- In order to understand whether climate change influenced not only the meteorological drought (i.e. low rainfall), but also other aspects of the drought, including the agricultural drought which influences how much water is available for plants, we also looked at the role of temperature. To do this we combined the rainfall assessment with an assessment of changes in potential evapotranspiration, i.e. how much water evaporates from soil and plants because of higher temperatures, in a multivariate analysis for the 24 months of drought.
- We found that, as a result of human-induced climate change, the combination of low rainfall and high evapotranspiration as unusual as the recent conditions would not have led to drought at all in a 1.2°C cooler world (see figure 2). In today's climate the same event is now classified as an exceptional drought (D4, dark red in fig. 1), with major crop and pasture losses and widespread water shortages. This change in drought severity is primarily due to the strong increase in evaporative demand caused by higher temperatures.
- Climate change has made events like the current drought much stronger and more likely; a conservative estimate is that such droughts have become about 100 times more likely.
- Fundamental to food security, health, and income, households engaged in rain-fed agriculture, agropastoralism, and pastoralism are vulnerable to drought and are among the most severely impacted groups when crop and livestock health decline. When rains fail these households are are forced to spend their limited assets on buffering losses and damages, and are consequently pushed further into poverty. State fragility and conflict, as well as the length of the drought played a significant role in worsening outcomes, especially for people in Somalia. Further, the severity of impacts linked to the long duration of the drought also raises serious questions about the length of droughts that government drought management systems and the international aid infrastructure should be prepared to handle in the future.
- The results of the study, coupled with climate projections indicating high confidence of increased heavy precipitation and pluvial floods in the north eastern Africa region (IPCC AR6), is illustrative of the myriad of climate impacts that people and governments in this region are confronted with. Taken together, regional climate variability and the projections indicate the need to invest in adaptation strategies that are robust to both wet and dry extremes, and which can be iterated upon as climate signals emerge and future projections become more certain.

https://doi.org/10.25561/102624

1 Introduction

The catastrophic impacts of the recurrent droughts in East Africa continue to worsen. Extended dry conditions punctuated by short intense rainfall events have become commonplace in the region (OCHA, 2023; Kimutai et al. 2022). The vagaries of extremes have substantially increased vulnerability and lowered the adaptive capacity of both human and environmental systems in the region. The below-average rainfall in the October-December (OND) 2022 season "short rains" made it the fifth consecutive failed season since OND 2020. The drought has been reported as the worst in 40 years (WMO, 2022, FAO 2022). Over the period, the persistent drought conditions have threatened people's livelihoods, increased the risk of disease, malnutrition, hunger and death, and fueled conflict and migration (MPI, 2023). It has led to substantial harvest failure, poor pasture conditions, livestock losses, decreased surface water availability and human conflicts (WFP, 2022). At least 180,000 refugees from Somalia and South Sudan crossed into the drought-stricken areas of Kenya and Ethiopia (UNHCR, 2022).

In Kenya, the government declared a drought emergency in September 2021 (WFP, 2022). By December 2022 the drought situation remained critical (alert and alarm drought phases) in twenty (20) of the 23 Arid and Semi Arid counties. The number of people in need of humanitarian assistance stood at 4.35 million (NDMA,2022). Cases of acute malnutrition were reported among 942,000 children aged 6-59 months and 134,000 pregnant or lactating women (UNFPA, 2022). The number of livestock deaths rose to over 2.4 million. These animals are an essential source of livelihood for pastoral communities. By January 2023, close to 9,210 metric tonnes of food commodities had been distributed and USD 7.29 million cash-based transfers made (OCHA, 2023). On 28th February 2023, the government appropriated a further Ksh. 4 Billion (approx. USD 30 million) to the nation's drought alleviation programme (Kenya Gov, 2023). Irrespective of the reported rains in most parts of the country by the last Dekad of March (KMD, 2023), the drought conditions are not likely to recover quickly enough to see improvements in food security before mid-2023. In Ethiopia and Somalia, more than 1.7 million people have been forced to move due to the impacts of the drought (UNHCR), with at least 60,000 school drop-outs reported in Ethiopia. By December 2022, up to 7.1 million people in Somalia were at risk of acute malnutrition and in need of urgent humanitarian aid (OCHA, 2023). More than 1 million people had moved from their homes, a situation that is exacerbated by concurrent conflict/insecurity and disease outbreaks.

Across the region, drought and high food prices have weakened many people's ability to grow crops, raise livestock and buy food. In Ethiopia, drought-affected populations are leaving their homes in search of water and food or due to inter-community conflicts which are flaring up due to competition over scarce resources. Across the region, food insecurity is mobilising people to move elsewhere for food and other priority needs (UNHCR, 2023b). An Integrated Food Security Phase Classification (IPC) analysis from 13 December 2022 highlights the strong possibility of a famine between April and June 2023, if the next rainy season fails and if humanitarian assistance is not sustained. Over 8.4 million Somalis are expected to face crisis levels (IPC Phase 3) of acute food insecurity by June 2023, including 223,000 who could face catastrophic levels of extreme hunger (IPC Phase 5) (IPC, 2023a). 1.8 million children under the age of 5 are projected to be affected by acute food insecurity (IPC Phase 3) (IPC, 2023b). In Kenya, approximately 5.4 million people are expected to face acute food insecurity during the same time frame (IPC, 2023c).

The region of Eastern Africa experiences two distinct rainy seasons, known as the long rains (occurring from March to May) and the short rains (from October to December), which have significant effects on both the environment and society. East Africa has particularly experienced an increased frequency of

droughts in the MAM season over the past few decades (Nicholson 2017). Hoell and Funk (2014) and Funk et al. (2018) linked the drying trend in the period 1981-2016 to intensification of the Indian Ocean branch of the Walker Circulation associated with anomalous warming of north-western Pacific attributable to human influence. Liebmann et al. (2014) related the MAM 1979-2012 drying trend to increased sensitivity of weather systems as a result of human-induced high zonal SST gradient between Indonesia and the central Pacific. Lott et al. (2013) found the role of human influence on enhanced probability of rainfall deficit in MAM 2011 season. Marthews et al. (2015) and Uhe et al. (2017), however, found no anthropogenic influence on the drought events of MAM 2014, MAM and OND 2016 respectively, but could not rule out an influence on surface air temperature and net incoming radiation.

It is useful to distinguish between the climate change signals in the multi-year drought and those in the most recent long-rains and the short-rain seasons of 2021 & 2022, in order to understand the contributions of the individual rainfall seasons to the multi-year drought. In this regard, we choose three temporal definitions - (1) 2-year average rainfall[1], (2) Seasonal average rainfall in MAM, (3) Seasonal average rainfall in OND rains. All indices are averaged over the study domain. Additionally, we examine the contribution from Potential Evapotranspiration (PET; calculated using the approach developed by Thornthwaite (1948)), as changes in PET due to regional warming are known to exacerbate droughts in the different global regions (e.g., Schumacher et al., 2022; Arias et al., 2023). We choose the Thornthwaite approach for calculating PET because (i) this approach requires only temperature observations and (ii) we use these estimates for calculating the Standardised precipitation evapotranspiration index (SPEI) that considers only the relative temporal evolution of evapotranspiration and therefore not sensitive to the choice of PET estimation method (Ortiz-Gómez et al., 2022; Vicente-Serrano et al., 2010).

The top panel in Fig. 1 shows the drought classification maps for the East Africa region (6°S-15°N, 32.5°E-52.5°E), based on the 24-month standardised precipitation index (SPI) from Jan 2021-Dec 2022, and the 3-month SPI for the 2022 MAM and OND in the top row; the bottom row shows the equivalent classifications for SPEI, Vicente-Serrano et al., 2010, 2014), which also takes into account the PET. Both of these drought indices are standardised with respect to 1980-2010 climatology. The colour scheme reflects the US Drought Monitor drought classifications (D0 - abnormally dry, D1 - moderate, D2 - severe, D3 - extreme, and D4 - exceptional). While the meteorological drought is exceptional only in the western part of the region (top row), the two-year agricultural drought is exceptional across much of the region (bottom row). Most of East Africa is found to have been under moderate to exceptional drought during the 2022 MAM season. Although there seems to have been a recovery in the subsequent OND season, parts of eastern Kenya, lowlands of Ethiopia and northeastern Somalia are still under drought.

For the remainder of the study, we compute these climate variables over a fairly homogeneous region, both in terms of elevation and climate (see Fig. A1 in the appendix). This region is outlined in black in Fig. 1, and hereafter referred to as EA. Such a selection is necessary because regions to the west and north of the proposed region do not have the distinct long and short rain seasons (see Fig. A2). It is worth noting that the proposed study domain encompasses the region

[1] 24-month precipitation was chosen in preference to a 30-month precipitation in order to disentangle the contribution of the long and short rain seasons, which would be less straightforward in a five-season period with two long and three short rains.

https://doi.org/10.25561/102624

over which agricultural impacts (crop harvest loss and pasturelands drying up) were reported (Paul, 6 July 2022).

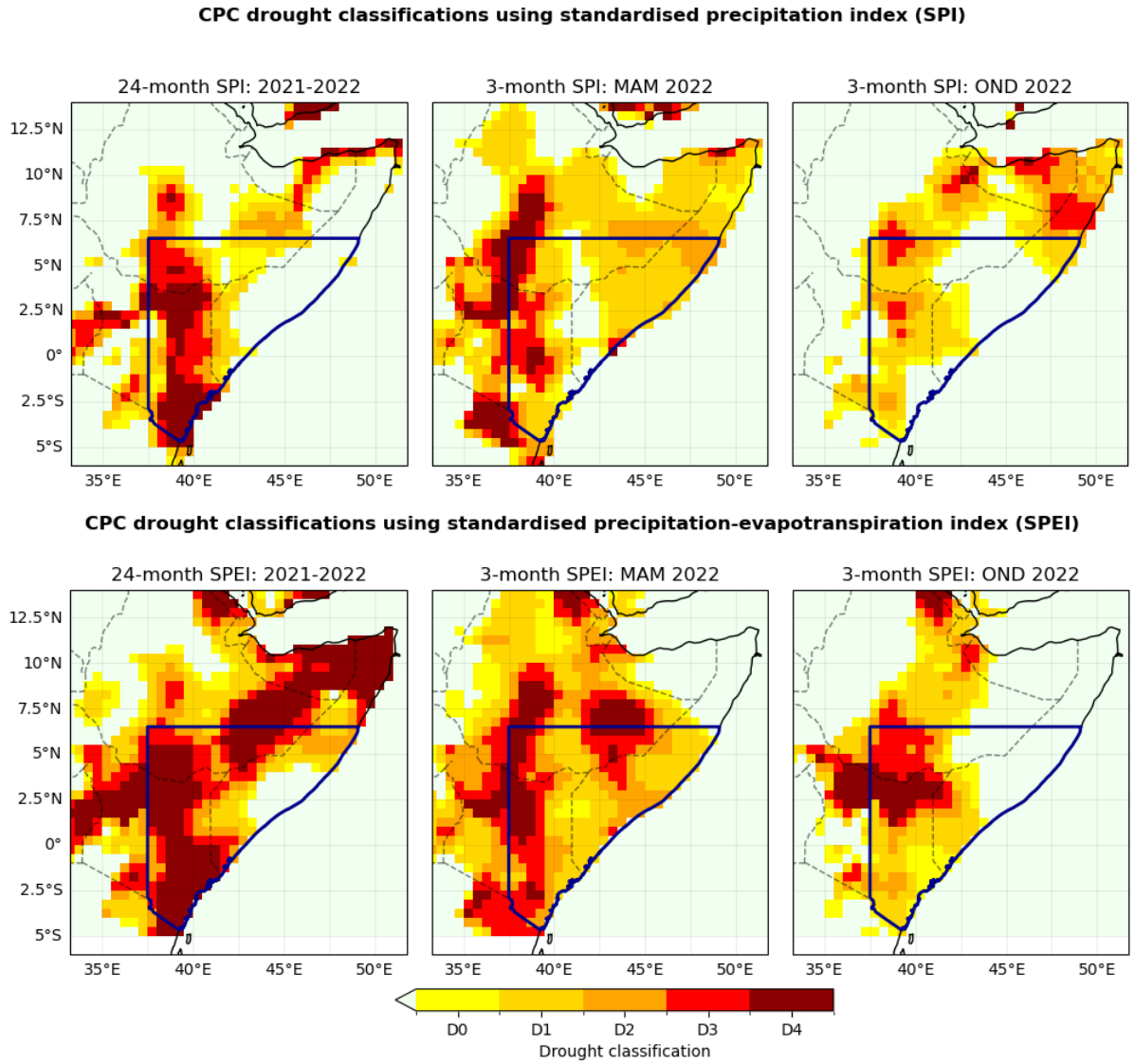

Figure 1: Top*: Drought classifications based on Standardised Precipitation Index (SPI; US Drought Monitor, 2023), reflecting the magnitudes of precipitation deficit from Jan 2021-Dec 2022 (left), from March-May 2022 (middle), and from Oct-December 2022 (right) relative to the 1980-2010 climatology in the CPC dataset.* ***Bottom****: Drought classifications based on Standardised Precipitation Evapotranspiration Index (SPEI), reflecting the magnitudes of precipitation deficit from Jan 2021-Dec 2022 (left), from March-May 2022 (middle), and from Oct-December 2022 (right) relative to the 1980-2010 climatology in the CPC dataset. The bold black outline highlights the study region.*

2 Data and methods

2.1 Observational data

The first dataset that we use in this study is the gridded product from NOAA PSL, Boulder, Colorado, USA known as the CPC Global Unified Daily Gridded data, available from their website. This data is

available at 0.5° x 0.5° resolution, for the period 1979-present. This source has both rainfall and mean temperature; therefore we use this as the primary dataset for this study.

The second gridded dataset is a combination of two datasets: CHIRPS (Climate Hazards Group InfraRed Precipitation with Station data; Funk et al., 2015b) and CenTrends (Centennial Trends; Funk et al., 2015a). CHIRPS is the state of the art observational daily dataset developed by the UC Santa Barbara Climate Hazards Group called "Climate Hazards Group InfraRed Precipitation with Station data" for East Africa available for the period 1981–present. CenTrends, on the other hand, is a monthly dataset, available for 1900–2014. CenTrends and CHIRPS are based on a similar assimilation technique and underlying observational data for their overlap period (1981-2014). They are highly correlated, with correlations over 0.95, justifying the extension of the CenTrends data
set from 1900-2014 with monthly averaged data from CHIRPS from 2015 onward.

As a measure of the El Niño - Southern Oscillation cycle (ENSO) we use the relative Nino3.4 index as defined in Van Oldenborgh et al., 2021. This is the Nino3.4 index (average SST over 5° S–5° N, 120°–170° W) minus the SST between 20° S–20° N to adjust the index for climate change. Because we are averaging the index over a period of several months, the values are not standardised per calendar month.

Finally, as a measure of anthropogenic climate change we use the (low-pass filtered) 4-year smoothed global mean surface temperature (GMST), where GMST is taken from the National Aeronautics and Space Administration (NASA) Goddard Institute for Space Science (GISS) surface temperature analysis (GISTEMP; Hansen et al., 2010; Lenssen et al. 2019).

Time series of precipitation from five stations within the study region were used to validate the gridded data products, by comparing the station data with the equivalent time series from the closest cell in the gridded dataset. Maps of the locations of the selected stations and comparison plots can be found in Figures A3 and A4. The CPC dataset was found to more accurately replicate the station time series than CenTrends/CHIRPS, supporting the choice of CPC as the primary data source in this study.

2.2 Model and experiment descriptions

We use four multi-model ensembles from climate modelling experiments using very different framings (Philip et al., 2020): Sea Surface temperature (SST) driven global circulation high resolution models, coupled global circulation models and regional climate models.

1. Coordinated Regional Climate Downscaling Experiment (CORDEX)-Africa (0.44° resolution, AFR-44) multi-model ensemble (Nikulin et al., 2012), comprising of 29 simulations resulting from combinations of 12 Global Climate Models (GCMs) and 8 Regional Climate Models (RCMs). These simulations are composed of historical simulations up to 2005, and extended to the year 2100 using the RCP8.5 scenario.

2. Coordinated Regional Climate Downscaling Experiment (CORDEX)-Africa (0.22° resolution, AFR-22) multi-model ensemble (Gutowski et al., 2016; Giorgi et al., 2021), comprising 10 simulations resulting from combinations of 5 GCMs and 4 RCMs. These simulations are composed of historical simulations up to 2005, and extended to the year 2100 using the RCP8.5 scenario.

3. The FLOR (Vecchi et al. 2014) and AM2.5C360 (Yang et al. 2021, Chan et al. 2021) climate models are developed at Geophysical Fluid Dynamics Laboratory (GFDL). The FLOR model is an atmosphere-ocean coupled GCM with a resolution of 50 km for land and atmosphere and 1 degree for ocean and ice. Ten ensemble simulations from FLOR are analysed, which cover the period from 1860 to 2100 and include both the historical and RCP4.5 experiments driven by transient radiative forcings from CMIP5 (Taylor et al. 2012). The AM2.5C360 is an atmospheric GCM based on that in the FLOR model (Delworth et al. 2012, Vecchi et al. 2014) with a horizontal resolution of 25 km. Three ensemble simulations of the Atmospheric Model Intercomparison Project (AMIP) experiment (1871-2050) are analysed. These simulations are initialised from three different pre-industrial conditions but forced by the same SSTs from HadISST1 (Rayner et al. 2003) after groupwise adjustments (Chan et al. 2021) over 1871-2020. SSTs between 2021 and 2050 are using the FLOR RCP4.5 experiment 10-ensemble mean values after bias correction. Radiative forcings are using historical values over 1871-2014 and RCP4.5 values after that.

4. HighResMIP SST-forced model ensemble (Haarsma et al. 2016), the 11 simulations of which span from 1950 to 2050. The SST and sea ice forcings for the period 1950-2014 are obtained from the 0.25° x 0.25° Hadley Centre Global Sea Ice and Sea Surface Temperature dataset that have undergone area-weighted regridding to match the climate model resolution (see Table B). For the 'future' time period (2015-2050), SST/sea-ice data are derived from RCP8.5 (CMIP5) data, and combined with greenhouse gas forcings from SSP5-8.5 (CMIP6) simulations (see Section 3.3 of Haarsma et al. 2016 for further details).

2.3 Statistical methods

In this analysis we use time series of precipitation and PET, area averaged over the EA study region (shown in Fig. 1), using reliable observational datasets and climate model simulations. Methods for observational and model analysis and for model evaluation and synthesis are used according to the World Weather Attribution Protocol, described in Philip et al. (2020), with supporting details found in van Oldenborgh et al. (2021), Ciavarella et al. (2021) and here.

The analysis steps include: (i) trend calculation from observations; (ii) model evaluation; (iii) multi-method multi-model attribution and (iv) synthesis of the attribution statement.
We calculate the return periods, Probability Ratio (PR; the factor-change in the event's probability) and change in intensity of the event under study in order to compare the climate of now and the climate of the past, defined respectively by the GMST values of now and of the preindustrial past (1850-1900, based on the Global Warming Index). To statistically model the event under study, we use Gaussian distributions fitted to the base-10 logarithm of precipitation (henceforth log10(precip); this distribution scales with GMST) and to the PET (distribution shifted with GMST). To account for potentially conflicting trends in the MAM and the OND rainfall due to regional warming and teleconnection patterns, we supplement the above approach with additional analyses in an effort to isolate the climate change signal from other confounding effects.

2.3.1. Exceptions in methods

1. **Analysis of 24-month rainfall and drought severity** - Previous studies examining changes in precipitation and temperature over East Africa found that although both variables have been increasing over this region, and are expected to continue to rise under future warming, the

severity of droughts in this region is exacerbated by increasing temperatures via increased PET (Haile et al., 2020; Nguvava et al., 2019). Therefore, for the attribution analysis of the 2021/2022 multi-year drought in this study, we supplement the standard univariate analysis of the 24-month precipitation by considering joint changes in the 24-month precipitation and PET using copulas, following Zachariah et al., 2023 and Zscheischler and Lehner, 2022).

(i) We fit Gaussian distributions that scale and shift with GMST to the base-10 logarithm of observed 24-month precipitation (X) and the PET (Y) time series respectively:

$$X \sim normal(\mu_X, \sigma_X, \alpha_X) \quad \text{and} \quad Y \sim normal(\mu_Y, \sigma_Y, \alpha_Y).$$

(ii) We use the cumulative distribution functions (CDFs) of these two distributions to compute the probabilities u and v of exceeding the values observed at each time t, so that

$$u_t = P(X \leq x_t) \quad \text{and} \quad v_t = 1 - P(Y \leq y_t)$$

Note that, because we are interested in the lower tails of the precipitation distribution and the upper tails of the PET distribution, these exceedance probabilities are given by the CDF of X and 1 - the CDF of Y.

(ii) The joint cumulative distribution function C is estimated from the marginal exceedance probabilities u and v by fitting a stationary Student's-t copula such that $C(\{u\},\{v\}) = P(\{U \leq u\},\{V \leq v\})$ for all (u, v) pairs (Nelsen, 2006)

(iv) Contours can be plotted over the subset $\{u, v\} \subset \{U, V\}$ - and therefore over the subset $\{x, y\} \subset \{X, Y\}$ - that share the same joint exceedance probability p, where $1/p$ is the return period of the event.

(v) The univariate distributions fitted in Step (i) are used to transform the (u,v) pairs to their equivalent return levels in the current climate and in a 1.2°C cooler climate in order to obtain joint return period contours for the current and pre-industrial climates.

2. **Attribution analysis of OND rainfall** - OND rainfall in eastern and southern Africa are known to be influenced by the phase of ENSO (Ogallo, 1997, 1998; Mutai and Ward 2000, Amissah-Arthur et al., 2002; Lott et al., 2011). We fitted linear regression models to the OND precipitation in the study region from CPC, CHIRPS and CenTrends-CHIRPS datasets, for two statistical models:
(i) log10precip depends on GMST (Model 1, Table A1). Here, while all datasets show a linearly increasing response to GMST, the trends are not statistically significant.

(ii) log10precip depends on GMST and Nino3.4 (Model 2, Table A1). As expected, the rainfall shows strong sensitivity to Nino3.4 (statistically significant trend at 5% significance level) in both datasets. The sensitivity of rainfall to GMST is also found to be higher than in Model 1, and statistically significant in the longer CenTrends-CHIRPS dataset.

To determine whether there is a climate change signal in the OND precipitation, we need to first disentangle the effects of ENSO and GMST. Therefore, the standard WWA method is amended in this case to include both NINO3.4 (detrended using tropical SSTs and averaged over OND) and GMST as covariates when fitting the distribution, so that
$log10\ pr \sim normal(\mu, \sigma \mid \mu_0, \sigma_0, \alpha, \beta)$.

Maximum likelihood estimation is used to estimate the model parameters, with

$$\mu = \mu_0 exp\left(\frac{\alpha T + \beta N}{\mu_o}\right) \quad \text{and} \quad \sigma = \sigma_0 exp\left(\frac{\alpha T + \beta N}{\mu_o}\right),$$

where T is the smoothed GMST, N is the Nino3.4 for OND, μ_0 and σ_0 are the mean and variance parameters of the nonstationary distribution and α, β are the trends due to GMST and Nino3.4, respectively. This formulation is used to ensure that the distribution has fixed dispersion. During attribution, the distribution is evaluated with N fixed at the 2022 value in both the current and 1.2°C cooler climate distributions, in order to obtain the change in likelihood and intensity of the 2022 OND low rainfall event due to climate change under the 2022 Nino conditions.

3 Observational analysis: return period and trend

3.1 Analysis of gridded data

3.1.1 24-month precipitation and SPEI

Figure 2 shows the trend-fitting results for the mean 24-month precipitation over the study region. While the shorter CPC dataset shows a decreasing trend (top left panel), the trend tends to slightly increase in the CenTrends-CHIRPS dataset (bottom left panel). This difference in trends can be ascribed to the differences in (i) data lengths of these datasets (44 years of CPC as compared to 122 years in CenTrends-CHIRPS) and (ii) trends and variability in the two contributing phenomena, namely, the MAM and OND rains. The right-hand panels show the return period curves for the variable in the current 2022 climate and a past counterfactual climate that would have been 1.2°C cooler. The best estimate of the return period for the 24-month low precipitation event ending in 2022 is found to be roughly 20 years in both datasets. The event is found to have been made 2 times more likely (uncertainty: 0.1 to 360) and 7% drier (uncertainty: 31% drier to 21% wetter) by climate change in the CPC dataset (top right panel). The results based on CenTrends-CHIRPS dataset (bottom right), on the other hand, show the drought to have become less likely (PR=0.7 uncertainty: 0.1 to 5) and 3% wetter (uncertainty: 12% drier to 19% wetter). It is noted that the uncertainties are high around these estimates.

Considering the role of increased PET associated with regional warming in amplifying drought impacts - especially agriculture due to changes in soil moisture and evapotranspiration rates - we also compute the trends and climate change signals in the 24-month SPEI. The observed SPEI value in the CPC dataset is -2.6, corresponding to an exceptional drought; the return period of this event in the current climate is about 10 years (Fig. A5). The climate change signal is much stronger, with the event made 5500 times (uncertainty: 32 to 4e+08) more likely and made more severe by 2.4 SPEI units (uncertainty: -4.7 to -1.2); in other words, a 1-in-10 year drought event in a world without climate change would be expected to have an SPEI of 0.3 (uncertainty: -1.4 to 2.1), corresponding to normal conditions with respect to the 1980-2010 climatology or, in the worst case, a drought classification of D0 (abnormally dry conditions).

Figure 3 shows the joint distribution of the 24-month precipitation and PET, along with the corresponding SPEI drought classification for each pair of values. The joint contours show that the probability of this particular combination of precipitation and PET in any given year in the 2022 climate is 1 in 26. The plot also highlights how unlikely the event would have been to occur in a 1.2°C cooler

climate, with the magenta point marking the 2022 event lying very far from the contours of the joint distribution in a cooler climate.

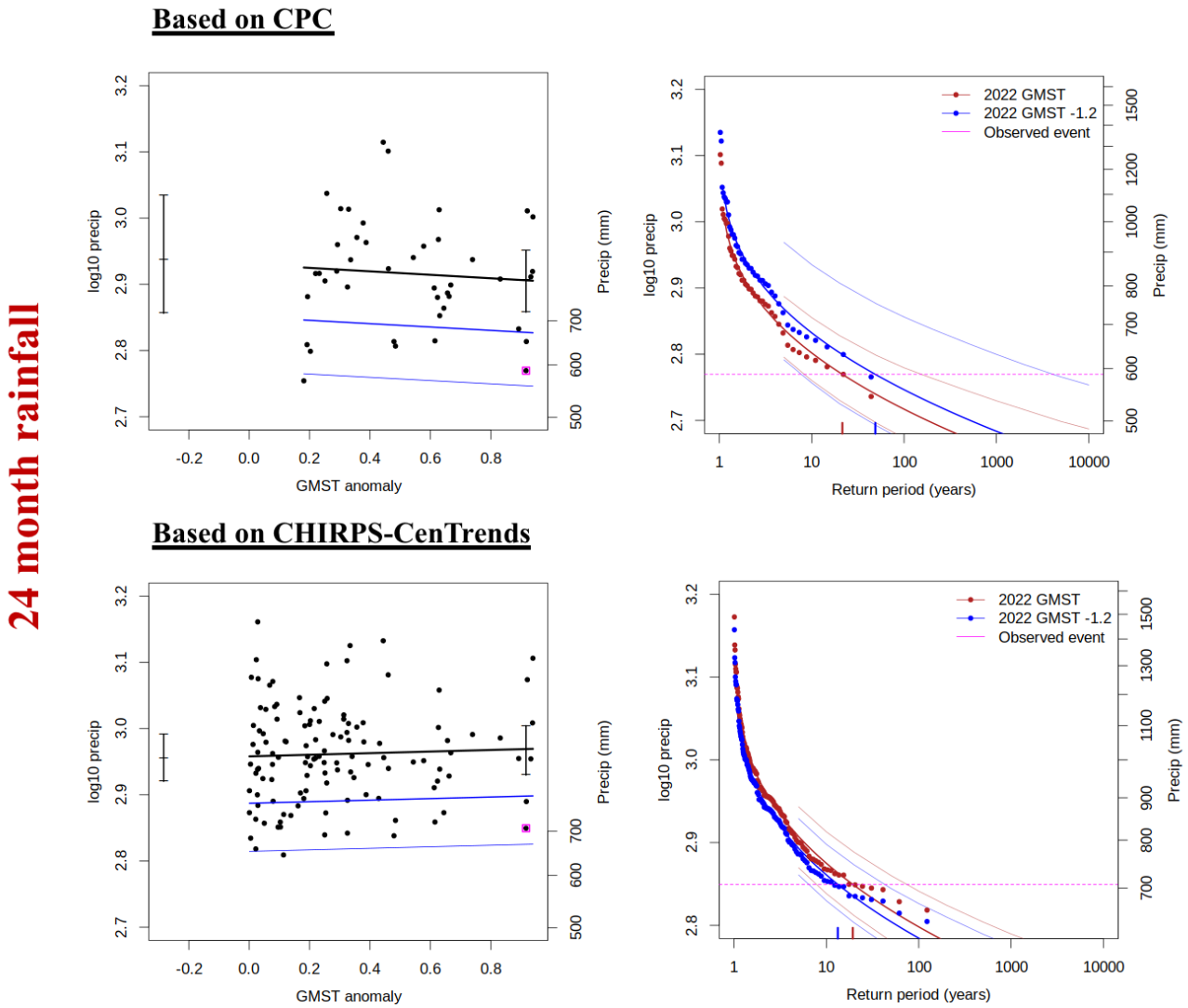

Figure 2: ***Left (top):*** *Response of 24-month rainfall (log-transformed and averaged over the study region) to change in global mean temperature, based on the CPC dataset. The thick black line denotes the time-varying mean, and the blue lines show 1 standard deviation (s.d) and 2 s.d below. The vertical black lines show the 95% confidence interval for the location parameter, for the current, 2022 climate and the hypothetical, 1.2ºC cooler climate. The average 24-month rainfall from Jan 2021-Dec 2022 is highlighted with the magenta box.* ***Right (top):*** *Gaussian-based return periods of log-transformed rainfall for the 2022 climate (red lines) and the 1.2ºC cooler climate (blue lines with 95% CI), based on CenTrends-CHIRPS dataset.* ***Left (bottom):*** *same as Left (top), based on CPC dataset.* ***Right (bottom):*** *same as Right (top), based on CHIRPS-CenTrends dataset.*

https://doi.org/10.25561/102624

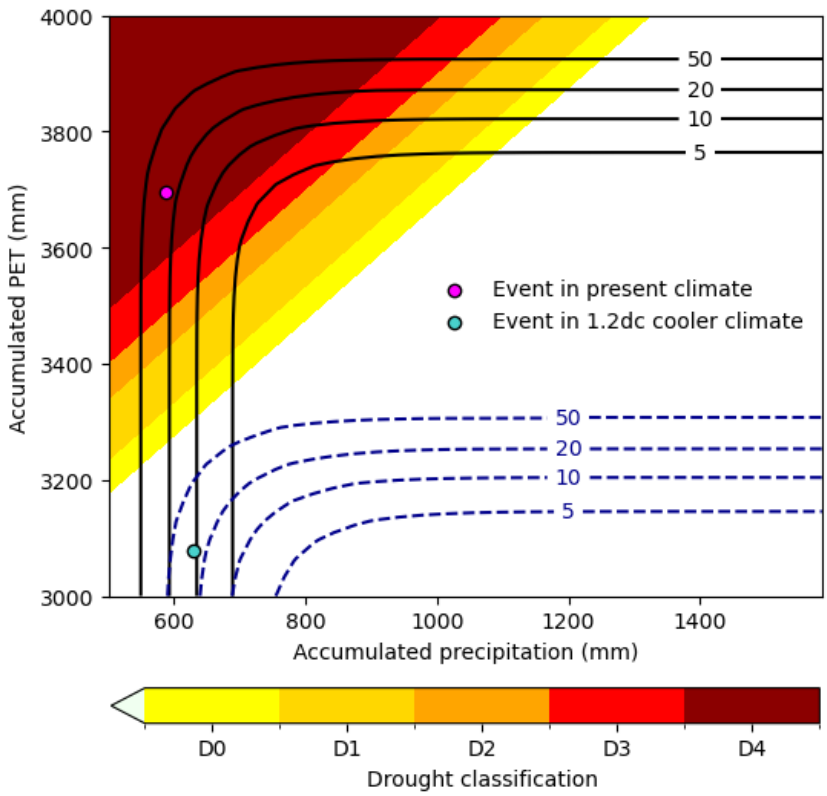

Figure 3: *Joint distribution of 24-month precip and PET with corresponding SPEI drought classification (CPC dataset). The solid contours indicate return periods under the joint distribution in the current climate, while the dashed contours indicate the same return periods in a 1.2°C cooler climate. The shaded contours represent different levels of drought severity. The magenta point indicates the 2022 drought event in the current climate, with a joint return period of 26 years (uncertainty: 23-37 years), while the turquoise point shows an event of the equivalent severity in a 1.2°C cooler climate.*

3.1.2 MAM precipitation

Figure 4 shows the trend-fitting results for the MAM precipitation, averaged over the study region, in CPC and CenTrends-CHIRPS. The left-hand panels show the log-transformed variable as a function of the GMST anomaly, while the right-hand panels show the Gaussian distribution-based return period curves for the log-transformed variable in the 2022 climate (red lines) and a past climate when the global mean temperature would have been 1.2°C cooler (blue lines). While there is a tendency towards decreasing rainfall with GMST rise in both datasets (left-hand panels), the trend is stronger in CPC, which may be ascribed to its shorter length and higher variability, which also results in larger uncertainty. The best estimates of the return period of the 2022 event are 11 and 6 years, for the respective datasets (right-hand panels). We round these to an average of 10 years for the attribution analysis. The 2022 MAM level is found to be 7 times (uncertainty: 0.2 to 3600) and 2 times (uncertainty: 0.4 to 8) more likely in the 2022 climate, from the CPC and CenTrends-CHIRPS, respectively. The respective intensity changes are -26% (uncertainty: -60% to 25%) and -8% (uncertainty: -31% to 17%), implying that the 2022 drought was drier due to climate change.

https://doi.org/10.25561/102624

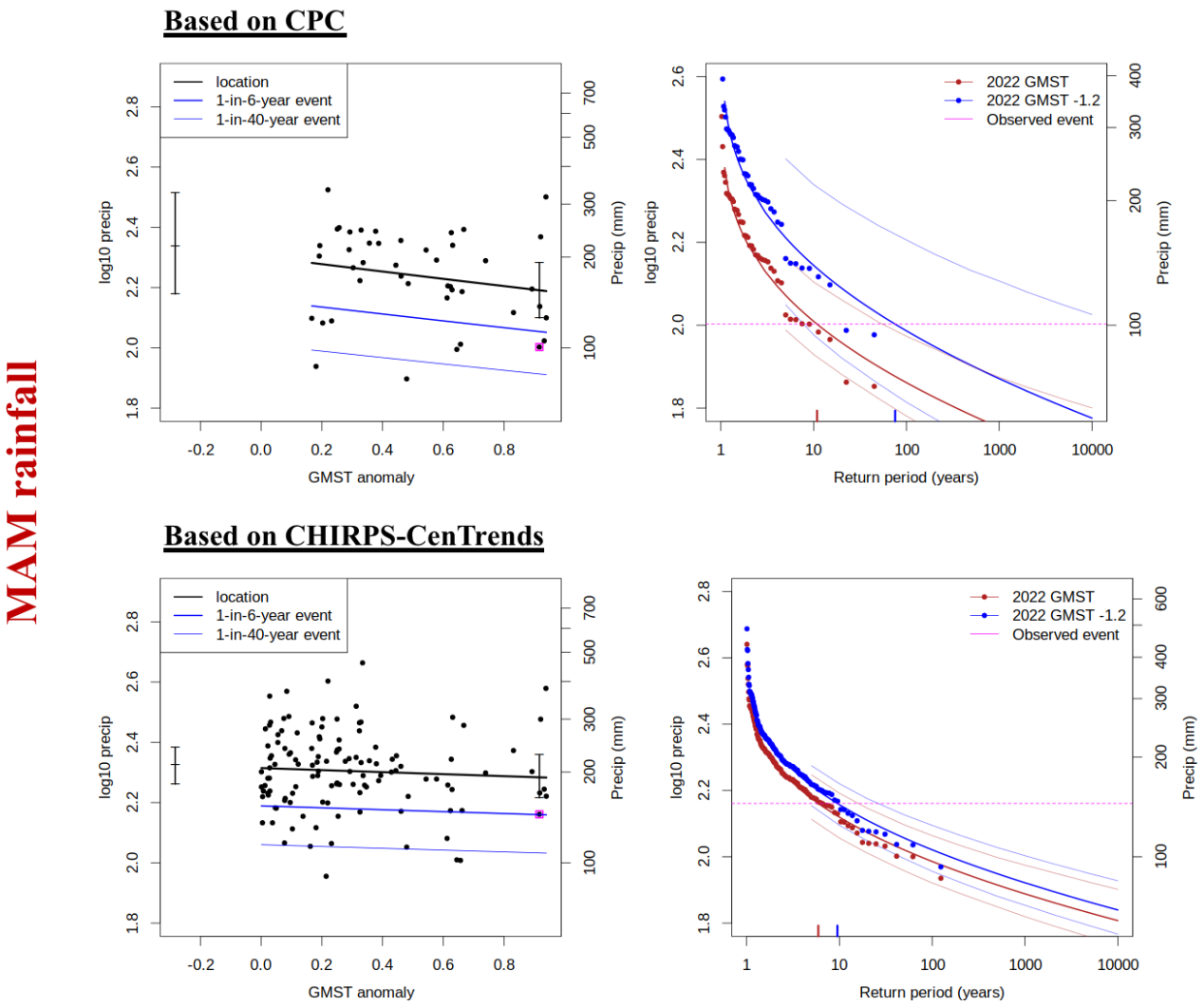

Figure 4: Left (top): *Response of MAM rainfall (log-transformed), averaged over the study region to change in global mean temperature, based on CPC dataset. The thick black line denotes the time-varying mean, and the blue lines show 1 standard deviation (s.d) and 2 s.d below. The vertical black lines show the 95% confidence interval for the location parameter, for the current, 2022 climate and the hypothetical, 1.2ºC cooler climate. The 2022 observation is highlighted with the magenta box.* ***Right (top):*** *Gaussian-based return periods of log-transformed rainfall for the 2022 climate (red lines with 95% CI) and the 1.2ºC cooler climate (blue lines with 95% CI), based on CenTrends-CHIRPS dataset.* ***Left (bottom):*** *same as Left(top), based on CPC dataset.* ***Right (bottom):*** *same as Right(top), based on CHIRPS-CenTrends dataset.*

3.1.3 OND precipitation

Fig. 5 shows similar plots for OND precipitation, but conditioned on the 2022 OND NINO3.4 (see (ii) in Section 2.3.1 for details). Despite differences between the datasets, both provide evidence of an increasing trend in the observations of OND precipitation in this region (left-hand panels in Fig. 5). The return period of the 2022 event in the current climate is estimated at 7 and 3 years in the CPC and CenTrends-CHIRPS datasets respectively (right-hand panels in Fig. 5), which are averaged to 5 years for the attribution analysis. The best estimates for the PR are less than 1 in both datasets, with PR = 0.3 (uncertainty: 0.06 to 2) in CPC and PR = 0.5 (uncertainty: 0.2 to 1) in CenTrends-CHIRPS, suggesting that drought in the short rain season has been made less likely due to climate change. The intensity changes also suggest that OND precipitation has increased by around 39% (uncertainty: -17% to 121%) and 30% (uncertainty: -3% to 70%).

https://doi.org/10.25561/102624

On comparing the above results with the fitted trends using only GMST as covariate, we find that the response to GMST is weaker when the ENSO effect is not taken into account (see left-hand panel, Fig. A6), possibly due to confounding effects of ENSO (as demonstrated in Table A1): in particular, the occurrence of three consecutive La Niña years at the end of the time series masks the underlying GMST trend to some extent. La Niña is known to exert substantial influence on OND rainfall in EA, and has been associated with most recent intense drought events in EA (e.g., 2010-2011; Funk, 2011, 2016; Uhe et al., 2017). Furthermore, co-occurrence of La Niña with the negative phase of the Indian Ocean Dipole (IOD) has been found to exacerbate drought conditions (Schubert et al., 2016). The IOD phase was negative in the most part of 2021 and 2022 (BOM, 2022).

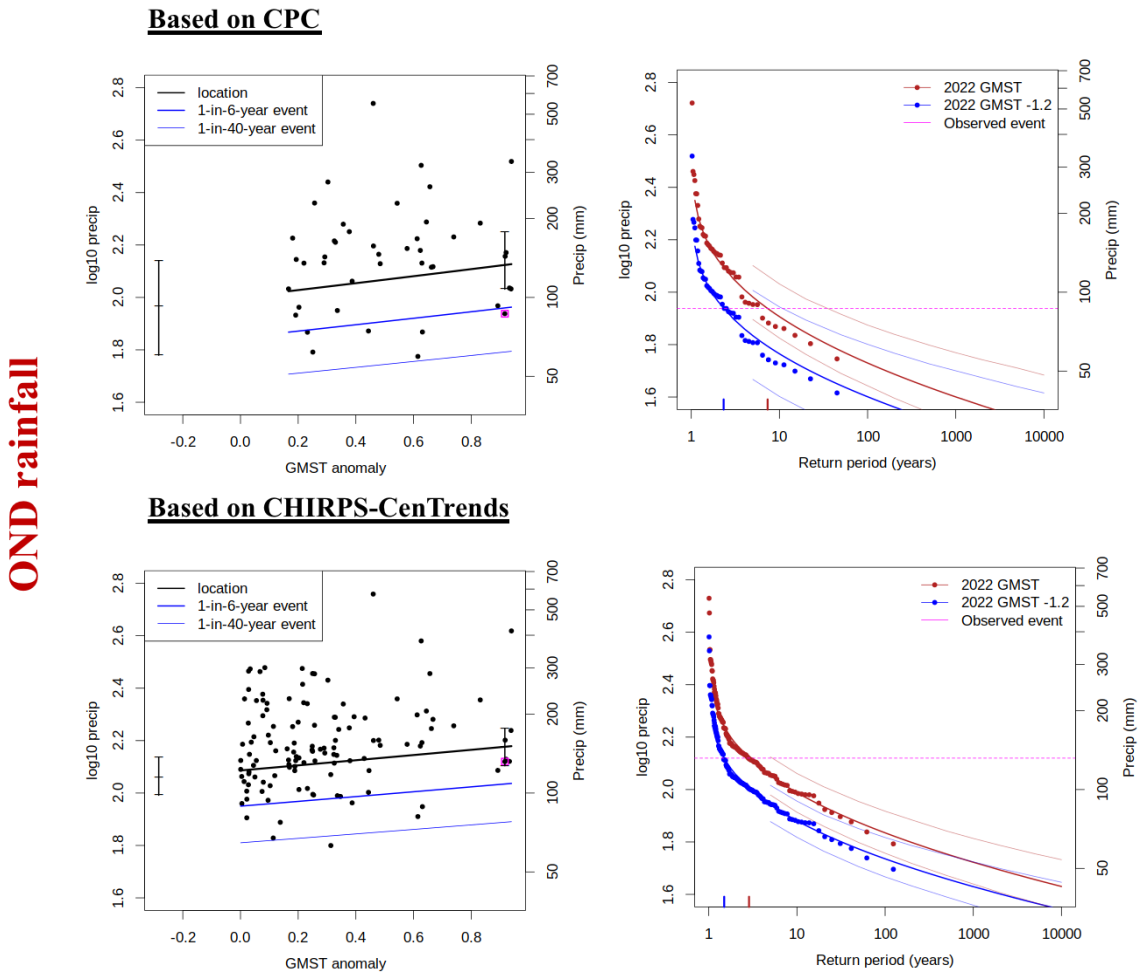

Figure 5: ***Left (top):*** *Response of OND rainfall (log-transformed), averaged over the study region to change in global mean temperature, based on the CPC dataset. The thick black line denotes the time-varying mean, and the blue lines show 1 standard deviation (s.d) and 2 s.d below. The vertical black lines show the 95% confidence interval for the location parameter, for the current, 2022 climate and the hypothetical, 1.2ºC cooler climate. The 2022 observation is highlighted with the magenta box.* ***Right (top):*** *Gaussian-based return periods of log-transformed rainfall for the 2022 climate (red lines) and the 1.2ºC cooler climate (blue lines with 95% CI), based on the CenTrends-CHIRPS dataset.* ***Left (bottom):*** *same as Left (top), based on the CPC dataset.* ***Right (bottom):*** *same as Right (top), based on the CHIRPS-CenTrends dataset.*

https://doi.org/10.25561/102624

4 Model evaluation

In the subsections below we show the results of the model evaluation for the EA region, for 24-month precipitation (Table 1), SPEI-24 (Table 2), MAM precipitation (Table 3), and OND precipitation (Table 4). Due to limitations in observed evapotranspiration products (discussed in Section 2), we do not evaluate the models for the effective precipitation. Instead, we choose those models that pass the evaluation for both precipitation and temperature for SPEI attribution analysis. Per framing or model setup we also use models that only just pass the evaluation tests if we only have five models or less for that framing that perform well. The tables show the model validation results. The climate models are evaluated against the observations in their ability to capture:

1. Seasonal cycles: For this, we qualitatively compare the model outputs against observations-based plots. We discard the models that fail to capture the bimodal seasonal cycle and/or exhibit ill-defined peaks in their seasonal cycles. We also discard the model if the rainy season onset/termination varies significantly from the observations.

2. Spatial patterns: Models that do not match the observations in terms of the large-scale precipitation patterns are excluded.

3. Parameters of the fitted models. We discard the model if the model and observation parameters ranges do not overlap. For distributions that scale with GMST (in this case, precipitation indices), the dispersion parameter is evaluated; for distributions that shift with GMST (in this case, SPEI), the variance parameter is evaluated.

The models are labelled as ‘good’, ’reasonable’, or ’bad’ based on their performances in terms of the three criteria discussed above.

Table 1: *Evaluation results for the climate models considered for the attribution analysis of* ***24-month precipitation for EA region****. The table contains qualitative assessments of seasonal cycle and spatial pattern of precipitation from the models (good, reasonable, bad) along with estimates for dispersion parameter and event magnitude. The corresponding estimates for observations are shown in blue. Based on overall suitability, the models are classified as good, reasonable and bad, shown by green, yellow and red highlights, respectively.*

Observations			**Dispersion**	**Event magnitude (mm)**
CPC			0.0280 (0.0212 ... 0.0328)	588
CenTrends + CHIRPS			0.0248 (0.0215 ... 0.0273)	707
Models	**Seasonal cycle**	**Spatial pattern**	**Dispersion**	**Threshold for 20-year event**
AFR-22_CanESM2_r1_CanRCM4 (1)	reasonable	good	0.0158 (0.0123 ... 0.0189)	926
AFR-22_HadGEM2-ES_r1_CCLM5-0-15 (1)	bad	reasonable	0.0357 (0.0276 ... 0.0420)	243
AFR-22_HadGEM2-ES_r1_RegCM4-7 (1)	bad	bad	0.0162 (0.0122 ... 0.0190)	871

AFR-22_HadGEM2-ES_r1_REMO2015 (1)	bad	reasonable	0.0227 (0.0180 ... 0.0259)	563
AFR-22_MPI-ESM-LR_r1_CCLM5-0-15 (1)	good	reasonable	0.0424 (0.0341 ... 0.0485)	402
AFR-22_MPI-ESM-LR_r1_REMO2015 (1)	reasonable	good	0.0268 (0.0213 ... 0.0308)	697
AFR-22_MPI-ESM-MR_r1_RegCM4-7 (1)	reasonable	good	0.0259 (0.0203 ... 0.0295)	809
AFR-22_NorESM1-M_r1_CCLM5-0-15 (1)	bad	reasonable	0.0258 (0.0203 ... 0.0298)	542
AFR-22_NorESM1-M_r1_RegCM4-7 (1)	bad	reasonable	0.0193 (0.0147 ... 0.0225)	1070
AFR-22_NorESM1-M_r1_REMO2015 (1)	bad	bad	0.0234 (0.0188 ... 0.0266)	695
AFR-44_CanESM2_r1_CanRCM4 (1)	good	bad	0.0168 (0.0132 ... 0.0199)	852
AFR-44_CanESM2_r1_RCA4 (1)	good	reasonable	0.0204 (0.0164 ... 0.0233)	555
AFR-44_CNRM-CM5_r1_CCLM4-8-17 (1)	reasonable	bad	0.0259 (0.0200 ... 0.0308)	649
AFR-44_CNRM-CM5_r1_RCA4 (1)	bad	bad	0.0263 (0.0186 ... 0.0312)	749
AFR-44_CSIRO-Mk3-6-0_r1_RCA4 (1)	good	good	0.0220 (0.0154 ... 0.0275)	359
AFR-44_EC-EARTH_r1_RACMO22T (1)	reasonable	bad	0.0138 (0.0107 ... 0.0160)	943
AFR-44_EC-EARTH_r1_RCA4 (1)	bad	bad	0.0178 (0.0143 ... 0.0202)	945
AFR-44_EC-EARTH_r12_CCLM4-8-17 (1)	good	bad	0.0295 (0.0227 ... 0.0347)	585
AFR-44_EC-EARTH_r12_RCA4 (1)	reasonable	bad	0.0136 (0.00974 ... 0.0169)	904
AFR-44_EC-EARTH_r12_REMO2009 (1)	reasonable	reasonable	0.0212 (0.0149 ... 0.0262)	729
AFR-44_EC-EARTH_r3_HIRHAM5 (1)	bad	reasonable	0.0204 (0.0164 ... 0.0233)	518
AFR-44_EC-EARTH_r3_RCA4 (1)	reasonable	bad	0.0164 (0.0133 ... 0.0184)	839
AFR-44_GFDL-ESM2M_r1_RCA4 (1)	bad	bad	0.0231 (0.0181 ... 0.0266)	834
AFR-44_HadGEM2-ES_r1_CCLM4-8-17 (1)	bad	reasonable	0.0350 (0.0267 ... 0.0415)	219
AFR-44_HadGEM2-ES_r1_RACMO22T (1)	bad	bad	0.0133 (0.0105 ... 0.0156)	739
AFR-44_HadGEM2-ES_r1_RCA4 (1)	bad	bad	0.0231 (0.0181 ... 0.0267)	575
AFR-44_HadGEM2-ES_r1_RegCM4-3 (1)	bad	reasonable	NA (NA ... NA)	NA

https://doi.org/10.25561/102624

AFR-44_HadGEM2-ES_r1_REMO2009 (1)	bad	reasonable	0.0244 (0.0196 ... 0.0277)	511
AFR-44_IPSL-CM5A-LR_r1_REMO2009 (1)	bad	reasonable	0.0208 (0.0157 ... 0.0245)	597
AFR-44_IPSL-CM5A-MR_r1_RCA4 (1)	reasonable	bad	0.0165 (0.0134 ... 0.0192)	868
AFR-44_MIROC5_r1_RCA4 (1)	good	reasonable	0.0169 (0.0133 ... 0.0193)	700
AFR-44_MIROC5_r1_REMO2009 (1)	bad	good	0.0252 (0.0201 ... 0.0286)	563
AFR-44_MPI-ESM-LR_r1_CCLM4-8-17 (1)	reasonable	bad	0.0458 (0.0365 ... 0.0520)	355
AFR-44_MPI-ESM-LR_r1_RCA4 (1)	reasonable	reasonable	0.0225 (0.0181 ... 0.0259)	828
AFR-44_MPI-ESM-LR_r1_REMO2009 (1)	reasonable	reasonable	0.0305 (0.0245 ... 0.0343)	583
AFR-44_MPI-ESM-LR_r2_RCA4 (1)	reasonable	bad	0.0138 (0.0112 ... 0.0159)	856
AFR-44_MPI-ESM-LR_r3_RCA4 (1)	reasonable	bad	0.0197 (0.0142 ... 0.0238)	809
AFR-44_MPI-ESM-MR_r1_RegCM4-3 (1)	reasonable	reasonable	-0.0344 (-0.0410 ... -0.0260)	0
AFR-44_NorESM1-M_r1_RCA4 (1)	bad	bad	0.0195 (0.0157 ... 0.0222)	751
CMCC-CM2-HR4 ()	good	reasonable	0.0119 (0.00893 ... 0.0140)	1328
CMCC-CM2-VHR4 ()	good	good	0.0140 (0.0100 ... 0.0169)	1807
CNRM-CM6-1-HR ()	reasonable	reasonable	0.0167 (0.0132 ... 0.0196)	931
CNRM-CM6-1 ()	reasonable	bad	0.0245 (0.0174 ... 0.0302)	732
EC-Earth3P-HR ()	reasonable	reasonable	0.0208 (0.0167 ... 0.0239)	598
EC-Earth3P ()	reasonable	good	0.0203 (0.0155 ... 0.0235)	734
HadGEM3-GC31-HM ()	reasonable	reasonable	0.0159 (0.0126 ... 0.0182)	934
HadGEM3-GC31-LM ()	good	bad	0.0207 (0.0162 ... 0.0240)	716
HadGEM3-GC31-MM ()	reasonable	bad	0.0216 (0.0170 ... 0.0247)	865
MPI-ESM1-2-HR ()	good	bad	0.0268 (0.0213 ... 0.0311)	452
MPI-ESM1-2-XR ()	good	bad	0.0282 (0.0224 ... 0.0325)	383
AM2.5 ()	reasonable	reasonable	0.0120 (0.0100 ... 0.0130)	*<not computed>*

https://doi.org/10.25561/102624

FLOR ()	reasonable	reasonable	0.015 (0.013 … 0.015)	*<not computed>*

Table 2**: same as Table 1 for **SPEI-24

Model / Observations			**Sigma**	**Event magnitude**
CPC			1.01 (0.785 ... 1.15)	(...)
Models	**Seasonal cycle**	**Spatial pattern**	**Sigma**	**Threshold for 10-year event**
AFR-22_CanESM2_r1_CanRCM4 (1)	bad	good	1.01 (0.799 ... 1.15)	-2.369
AFR-22_HadGEM2-ES_r1_CCLM5-0-15 (1)	bad	reasonable	1.17 (0.907 ... 1.32)	-2.728
AFR-22_HadGEM2-ES_r1_RegCM4-7 (1)	bad	bad	1.15 (0.932 ... 1.29)	-2.426
AFR-22_HadGEM2-ES_r1_REMO2015 (1)	bad	reasonable	1.32 (1.05 ... 1.51)	-3.161
AFR-22_MPI-ESM-LR_r1_CCLM5-0-15 (1)	good	reasonable	1.33 (1.01 ... 1.54)	-2.950
AFR-22_MPI-ESM-LR_r1_REMO2015 (1)	reasonable	good	1.30 (1.03 ... 1.49)	-3.587
AFR-22_MPI-ESM-MR_r1_RegCM4-7 (1)	bad	bad	1.08 (0.881 ... 1.21)	-1.892
AFR-22_NorESM1-M_r1_CCLM5-0-15 (1)	bad	reasonable	1.11 (0.888 ... 1.26)	-2.145
AFR-22_NorESM1-M_r1_RegCM4-7 (1)	bad	bad	1.25 (0.982 ... 1.43)	-2.400
AFR-22_NorESM1-M_r1_REMO2015 (1)	bad	bad	1.19 (0.919 ... 1.39)	-2.110
AFR-44_CanESM2_r1_CanRCM4 (1)	bad	bad	0.993 (0.781 ... 1.13)	-1.936
AFR-44_CanESM2_r1_RCA4 (1)	reasonable	reasonable	1.04 (0.878 ... 1.15)	-2.435
AFR-44_CNRM-CM5_r1_CCLM4-8-17 (1)	reasonable	bad	1.08 (0.832 ... 1.25)	-1.839
AFR-44_CNRM-CM5_r1_RCA4 (1)	bad	bad	1.09 (0.798 ... 1.30)	-1.395
AFR-44_CSIRO-Mk3-6-0_r1_RCA4 (1)	good	reasonable	1.21 (0.982 ... 1.35)	-2.593
AFR-44_EC-EARTH_r1_RACMO22T (1)	bad	bad	0.965 (0.728 ... 1.13)	-1.534
AFR-44_EC-EARTH_r1_RCA4 (1)	bad	bad	1.02 (0.730 ... 1.23)	-1.478
AFR-44_EC-EARTH_r12_CCLM4-8-17 (1)	good	bad	0.998 (0.818 ... 1.13)	-1.611

https://doi.org/10.25561/102624

AFR-44_EC-EARTH_r12_RCA4 (1)	bad	bad	1.22 (0.942 ... 1.42)	-2.292
AFR-44_EC-EARTH_r12_REMO2009 (1)	reasonable	reasonable	1.13 (0.851 ... 1.32)	-1.814
AFR-44_EC-EARTH_r3_HIRHAM5 (1)	bad	reasonable	1.13 (0.905 ... 1.28)	-2.712
AFR-44_EC-EARTH_r3_RCA4 (1)	bad	bad	1.11 (0.892 ... 1.25)	-2.178
AFR-44_GFDL-ESM2M_r1_RCA4 (1)	bad	bad	1.12 (0.855 ... 1.32)	-2.068
AFR-44_HadGEM2-ES_r1_CCLM4-8-17 (1)	bad	reasonable	1.20 (0.951 ... 1.35)	-3.020
AFR-44_HadGEM2-ES_r1_RACMO22T (1)	bad	bad	1.21 (0.956 ... 1.37)	-3.124
AFR-44_HadGEM2-ES_r1_RCA4 (1)	bad	bad	1.15 (0.923 ... 1.30)	-2.715
AFR-44_HadGEM2-ES_r1_RegCM4-3 (1)	bad	reasonable	NA (NA ... NA)	NA
AFR-44_HadGEM2-ES_r1_REMO2009 (1)	bad	reasonable	1.52 (1.19 ... 1.75)	-3.934
AFR-44_IPSL-CM5A-LR_r1_REMO2009 (1)	bad	reasonable	1.10 (0.925 ... 1.19)	-2.185
AFR-44_IPSL-CM5A-MR_r1_RCA4 (1)	bad	bad	1.13 (0.900 ... 1.31)	-2.517
AFR-44_MIROC5_r1_RCA4 (1)	good	reasonable	1.40 (1.09 ... 1.60)	-2.771
AFR-44_MIROC5_r1_REMO2009 (1)	bad	reasonable	1.48 (1.16 ... 1.71)	-3.407
AFR-44_MPI-ESM-LR_r1_CCLM4-8-17 (1)	reasonable	bad	1.17 (0.928 ... 1.33)	-2.764
AFR-44_MPI-ESM-LR_r1_RCA4 (1)	reasonable	reasonable	1.15 (0.881 ... 1.36)	-2.685
AFR-44_MPI-ESM-LR_r1_REMO2009 (1)	reasonable	reasonable	1.25 (1.01 ... 1.41)	-3.436
AFR-44_MPI-ESM-LR_r2_RCA4 (1)	reasonable	bad	0.990 (0.796 ... 1.12)	-2.473
AFR-44_MPI-ESM-LR_r3_RCA4 (1)	reasonable	bad	1.51 (1.15 ... 1.74)	-3.372
AFR-44_MPI-ESM-MR_r1_RegCM4-3 (1)	bad	reasonable	1.20 (0.995 ... 1.33)	-2.834
AFR-44_NorESM1-M_r1_RCA4 (1)	bad	bad	1.11 (0.898 ... 1.25)	-2.265
CMCC-CM2-HR4 ()	good	reasonable	1.06 (0.775 ... 1.32)	-2.621
CMCC-CM2-VHR4 ()	good	good	0.985 (0.759 ... 1.14)	-2.011
CNRM-CM6-1-HR ()	bad	bad	0.786 (0.631 ... 0.916)	-2.062

https://doi.org/10.25561/102624

CNRM-CM6-1 ()	reasonable	bad	0.838 (0.675 ... 0.948)	-2.059
EC-Earth3P-HR ()	reasonable	reasonable	0.743 (0.606 ... 0.841)	-2.463
EC-Earth3P ()	reasonable	good	0.795 (0.618 ... 0.904)	-2.310
HadGEM3-GC31-HM ()	reasonable	reasonable	0.692 (0.555 ... 0.781)	-2.647
HadGEM3-GC31-LM ()	good	bad	0.885 (0.697 ... 1.02)	-2.755
HadGEM3-GC31-MM ()	reasonable	bad	0.771 (0.619 ... 0.884)	-1.998
MPI-ESM1-2-HR ()	good	bad	1.03 (0.810 ... 1.19)	-2.024
MPI-ESM1-2-XR ()	good	bad	0.942 (0.716 ... 1.10)	-2.018

Table 3**: same as Table 1 for **MAM precipitation

Model / Observations	**Seasonal cycle**	**Spatial pattern**	**Dispersion**	**Event magnitude (mm)**
CPC			0.0647 (0.0488 ... 0.0762)	101
CHIRPS-CENTrends			0.0561 (0.0481 ... 0.0623)	145
Models	**Seasonal cycle**	**Spatial pattern**	**Dispersion**	**Threshold for 10-year event**
AFR-22_CanESM2_r1_CanRCM4 (1)	reasonable	good	0.0448 (0.0324 ... 0.0560)	926
AFR-22_HadGEM2-ES_r1_CCLM5-0-15 (1)	bad	reasonable	0.148 (0.107 ... 0.184)	243
AFR-22_HadGEM2-ES_r1_RegCM4-7 (1)	bad	bad	0.101 (0.0682 ... 0.132)	871
AFR-22_HadGEM2-ES_r1_REMO2015 (1)	bad	reasonable	0.104 (0.0757 ... 0.125)	563
AFR-22_MPI-ESM-LR_r1_CCLM5-0-15 (1)	good	reasonable	0.111 (0.0841 ... 0.128)	402
AFR-22_MPI-ESM-LR_r1_REMO2015 (1)	reasonable	good	0.0816 (0.0615 ... 0.0977)	697
AFR-22_MPI-ESM-MR_r1_RegCM4-7 (1)	reasonable	good	0.0784 (0.0645 ... 0.0877)	809
AFR-22_NorESM1-M_r1_CCLM5-0-15 (1)	bad	reasonable	0.131 (0.105 ... 0.146)	542
AFR-22_NorESM1-M_r1_RegCM4-7 (1)	bad	reasonable	0.112 (0.0893 ... 0.129)	1070
AFR-22_NorESM1-M_r1_REMO2015 (1)	bad	good	0.131 (0.0999 ... 0.154)	695

https://doi.org/10.25561/102624

AFR-44_CanESM2_r1_CanRCM4 (1)	good	bad	0.0445 (0.0320 ... 0.0553)	852
AFR-44_CanESM2_r1_RCA4 (1)	good	reasonable	0.0689 (0.0541 ... 0.0805)	555
AFR-44_CNRM-CM5_r1_CCLM4-8-17 (1)	reasonable	bad	0.124 (0.0966 ... 0.147)	649
AFR-44_CNRM-CM5_r1_RCA4 (1)	reasonable	good	0.0671 (0.0521 ... 0.0781)	749
AFR-44_CSIRO-Mk3-6-0_r1_RCA4 (1)	good	good	0.0746 (0.0474 ... 0.0981)	359
AFR-44_EC-EARTH_r1_RACMO22T (1)	reasonable	bad	0.0471 (0.0318 ... 0.0588)	943
AFR-44_EC-EARTH_r1_RCA4 (1)	good	good	0.0515 (0.0410 ... 0.0598)	945
AFR-44_EC-EARTH_r12_CCLM4-8-17 (1)	good	bad	0.0826 (0.0617 ... 0.0999)	585
AFR-44_EC-EARTH_r12_RCA4 (1)	good	good	0.0563 (0.0399 ... 0.0712)	904
AFR-44_EC-EARTH_r12_REMO2009 (1)	good	good	0.0962 (0.0676 ... 0.120)	729
AFR-44_EC-EARTH_r3_HIRHAM5 (1)	bad	good	0.114 (0.0855 ... 0.135)	518
AFR-44_EC-EARTH_r3_RCA4 (1)	reasonable	good	0.0640 (0.0469 ... 0.0757)	839
AFR-44_GFDL-ESM2M_r1_RCA4 (1)	bad	reasonable	0.0934 (0.0710 ... 0.111)	834
AFR-44_HadGEM2-ES_r1_CCLM4-8-17 (1)	bad	reasonable	0.136 (0.105 ... 0.158)	219
AFR-44_HadGEM2-ES_r1_RACMO22T (1)	bad	reasonable	0.0509 (0.0347 ... 0.0631)	739
AFR-44_HadGEM2-ES_r1_RCA4 (1)	bad	reasonable	0.0867 (0.0658 ... 0.102)	575
AFR-44_HadGEM2-ES_r1_REMO2009 (1)	bad	good	0.101 (0.0762 ... 0.120)	511
AFR-44_IPSL-CM5A-LR_r1_REMO2009 (1)	bad	reasonable	0.0925 (0.0731 ... 0.107)	597
AFR-44_IPSL-CM5A-MR_r1_RCA4 (1)	reasonable	good	0.0524 (0.0393 ... 0.0641)	868
AFR-44_MIROC5_r1_RCA4 (1)	good	reasonable	0.0463 (0.0343 ... 0.0547)	700
AFR-44_MIROC5_r1_REMO2009 (1)	good	good	0.0753 (0.0595 ... 0.0872)	563
AFR-44_MPI-ESM-LR_r1_CCLM4-8-17 (1)	reasonable	reasonable	0.119 (0.0909 ... 0.139)	355

https://doi.org/10.25561/102624

AFR-44_MPI-ESM-LR_r1_RCA4 (1)	reasonable	reasonable	0.0579 (0.0445 ... 0.0696)	828
AFR-44_MPI-ESM-LR_r1_REMO2009 (1)	reasonable	reasonable	0.0836 (0.0631 ... 0.0997)	583
AFR-44_MPI-ESM-LR_r2_RCA4 (1)	reasonable	reasonable	0.0481 (0.0364 ... 0.0575)	856
AFR-44_MPI-ESM-LR_r3_RCA4 (1)	reasonable	reasonable	0.0491 (0.0381 ... 0.0568)	809
AFR-44_NorESM1-M_r1_RCA4 (1)	bad	reasonable	0.108 (0.0822 ... 0.127)	751
CMCC-CM2-HR4 (1)	good	reasonable	0.0406 (0.0310 ... 0.0481)	1328
CMCC-CM2-VHR4 (1)	good	good	0.0511 (0.0398 ... 0.0588)	1807
CNRM-CM6-1-HR (1)	reasonable	reasonable	0.0635 (0.0517 ... 0.0717)	931
CNRM-CM6-1 (1)	reasonable	reasonable	0.0922 (0.0657 ... 0.115)	732
EC-Earth3P-HR (1)	reasonable	reasonable	0.0626 (0.0495 ... 0.0715)	598
EC-Earth3P (1)	reasonable	good	0.0672 (0.0498 ... 0.0817)	734
HadGEM3-GC31-HM (1)	reasonable	reasonable	0.0458 (0.0330 ... 0.0571)	934
HadGEM3-GC31-LM (1)	good	bad	0.0700 (0.0535 ... 0.0820)	716
HadGEM3-GC31-MM (1)	reasonable	bad	0.0593 (0.0490 ... 0.0667)	865
MPI-ESM1-2-HR (1)	good	bad	0.120 (0.0931 ... 0.144)	452
MPI-ESM1-2-XR (1)	good	bad	0.104 (0.0774 ... 0.124)	383
AM2.5 ()	reasonable	reasonable	0.0270 (0.0230 ... 0.0290)	<not computed>
FLOR ()	reasonable	reasonable	0.044 (0.041 …).047)	<not computed>

Table 4**: same as Table 1 for **OND precipitation

Model / Observations	Seasonal cycle	Spatial pattern	Dispersion	Event magnitude
CPC			0.0798 (0.0590 ... 0.0930)	87
CHIRPS-CENTrends			0.0675 (0.0571 ... 0.0763)	132
Models	**Seasonal cycle**	**Spatial pattern**	**Dispersion**	**Threshold for 5-year event**

https://doi.org/10.25561/102624

AFR-22_CanESM2_r1_CanRCM4 (1)	good	good	0.0365 (0.0266 ... 0.0426)	260
AFR-22_HadGEM2-ES_r1_CCLM5-0-15 (1)	bad	reasonable	0.0827 (0.0583 ... 0.0995)	24
AFR-22_HadGEM2-ES_r1_RegCM4-7 (1)	bad	reasonable	0.0433 (0.0343 ... 0.0493)	104
AFR-22_HadGEM2-ES_r1_REMO2015 (1)	bad	good	0.0810 (0.0578 ... 0.0977)	36
AFR-22_MPI-ESM-LR_r1_CCLM5-0-15 (1)	good	good	0.0887 (0.0669 ... 0.102)	78
AFR-22_MPI-ESM-LR_r1_REMO2015 (1)	reasonable	good	0.0741 (0.0546 ... 0.0893)	112
AFR-22_MPI-ESM-MR_r1_RegCM4-7 (1)	reasonable	good	0.0629 (0.0471 ... 0.0745)	235
AFR-22_NorESM1-M_r1_CCLM5-0-15 (1)	good	good	0.0675 (0.0500 ... 0.0810)	51
AFR-22_NorESM1-M_r1_RegCM4-7 (1)	good	bad	0.0369 (0.0281 ... 0.0433)	102
AFR-22_NorESM1-M_r1_REMO2015 (1)	bad	bad	0.0612 (0.0462 ... 0.0710)	48
AFR-44_CanESM2_r1_CanRCM4 (1)	good	bad	0.0377 (0.0262 ... 0.0446)	300
AFR-44_CanESM2_r1_RCA4 (1)	good	reasonable	0.0564 (0.0435 ... 0.0638)	160
AFR-44_CNRM-CM5_r1_CCLM4-8-17 (1)	reasonable	bad	0.0565 (0.0446 ... 0.0645)	81
AFR-44_CNRM-CM5_r1_RCA4 (1)	bad	bad	0.0617 (0.0498 ... 0.0683)	71
AFR-44_CSIRO-Mk3-6-0_r1_RCA4 (1)	good	good	0.0904 (0.0639 ... 0.109)	62
AFR-44_EC-EARTH_r1_RACMO22T (1)	good	bad	0.0383 (0.0283 ... 0.0444)	295
AFR-44_EC-EARTH_r1_RCA4 (1)	bad	bad	0.0509 (0.0377 ... 0.0606)	264
AFR-44_EC-EARTH_r12_CCLM4-8-17 (1)	good	bad	0.0827 (0.0572 ... 0.101)	209
AFR-44_EC-EARTH_r12_RCA4 (1)	reasonable	bad	0.0478 (0.0348 ... 0.0561)	231
AFR-44_EC-EARTH_r12_REMO2009 (1)	reasonable	reasonable	0.0626 (0.0434 ... 0.0769)	162
AFR-44_EC-EARTH_r3_HIRHAM5 (1)	reasonable	reasonable	0.0492 (0.0382 ... 0.0552)	183
AFR-44_EC-EARTH_r3_RCA4 (1)	reasonable	bad	0.0410 (0.0292 ... 0.0493)	219
AFR-44_GFDL-ESM2M_r1_RCA4 (1)	reasonable	bad	0.0579 (0.0415 ... 0.0717)	109

https://doi.org/10.25561/102624

AFR-44_HadGEM2-ES_r1_CCLM4-8-17 (1)	bad	reasonable	0.0907 (0.0641 ... 0.110)	22
AFR-44_HadGEM2-ES_r1_RACMO22T (1)	bad	bad	0.0363 (0.0271 ... 0.0416)	119
AFR-44_HadGEM2-ES_r1_RCA4 (1)	bad	bad	0.0658 (0.0505 ... 0.0751)	70
AFR-44_HadGEM2-ES_r1_REMO2009 (1)	bad	reasonable	0.105 (0.0809 ... 0.120)	32
AFR-44_IPSL-CM5A-LR_r1_REMO2009 (1)	bad	good	0.0795 (0.0572 ... 0.0975)	56
AFR-44_IPSL-CM5A-MR_r1_RCA4 (1)	good	bad	0.0438 (0.0344 ... 0.0498)	234
AFR-44_MIROC5_r1_RCA4 (1)	good	good	0.0610 (0.0471 ... 0.0695)	60
AFR-44_MIROC5_r1_REMO2009 (1)	bad	good	0.0727 (0.0554 ... 0.0843)	32
AFR-44_MPI-ESM-LR_r1_CCLM4-8-17 (1)	good	bad	0.0917 (0.0694 ... 0.105)	79
AFR-44_MPI-ESM-LR_r1_RCA4 (1)	reasonable	reasonable	0.0545 (0.0411 ... 0.0637)	146
AFR-44_MPI-ESM-LR_r1_REMO2009 (1)	reasonable	reasonable	0.0781 (0.0619 ... 0.0889)	75
AFR-44_MPI-ESM-LR_r2_RCA4 (1)	reasonable	bad	0.0435 (0.0341 ... 0.0495)	165
AFR-44_MPI-ESM-LR_r3_RCA4 (1)	reasonable	bad	0.0536 (0.0412 ... 0.0618)	180
AFR-44_NorESM1-M_r1_RCA4 (1)	good	bad	0.0473 (0.0340 ... 0.0573)	87
CMCC-CM2-HR4 (1)	good	reasonable	0.0311 (0.0202 ... 0.0399)	242
CMCC-CM2-VHR4 (1)	good	good	0.0368 (0.0271 ... 0.0452)	291
CNRM-CM6-1-HR (1)	reasonable	good	0.0401 (0.0305 ... 0.0465)	197
CNRM-CM6-1 (1)	reasonable	bad	0.0687 (0.0527 ... 0.0795)	134
EC-Earth3P-HR (1)	reasonable	reasonable	0.0642 (0.0472 ... 0.0750)	113
EC-Earth3P (1)	reasonable	good	0.0581 (0.0454 ... 0.0647)	139
HadGEM3-GC31-HM (1)	reasonable	reasonable	0.0383 (0.0278 ... 0.0457)	182
HadGEM3-GC31-LM (1)	good	bad	0.0512 (0.0376 ... 0.0602)	145
HadGEM3-GC31-MM (1)	reasonable	good	0.0495 (0.0402 ... 0.0554)	191
MPI-ESM1-2-HR (1)	good	bad	0.0785 (0.0559 ... 0.0950)	86

https://doi.org/10.25561/102624

MPI-ESM1-2-XR (1)	good	bad	0.0963 (0.0672 ... 0.121)	65
AM2.5 ()	reasonable	reasonable	0.0250 (0.0210 ... 0.0280)	<not computed>
FLOR ()	reasonable	reasonable	0.038 (0.035 … 0.041)	<not computed>

5 Multi-method multi-model attribution

This section shows Probability Ratios and change in intensity ΔI for models and also includes the values calculated from the observations.

Table 5: *Probability ratio and change in intensity in the* ***24-month precipitation*** *for models that passed the validation tests.*

Model / Observations	**a. Past vs. present**		**b. Present vs. future**	
	Probability ratio PR [-]	**Change in intensity ΔI [%]**	**Probability ratio PR [-]**	**Change in intensity ΔI [%]**
CPC	2.3 (0.090 ... 3.6e+2)	-6.7 (-31 ... 21)		
CenTrends + CHIRPS	0.69 (0.11 ... 4.5)	3.3 (-12 ... 19)		
AFR-22_MPI-ESM-LR_r1_REMO2015 (1)	0.16 (0.018 ... 0.62)	21 (5.9 ... 38)	0.93 (0.57 ... 1.3)	1.0 (-4.8 ... 6.5)
AFR-22_MPI-ESM-MR_r1_RegCM4-7 (1)	0.51 (0.076 ... 4.6)	6.3 (-11 ... 25)	0.39 (0.16 ... 0.74)	6.6 (2.3 ... 10)
AFR-44_CanESM2_r1_RCA4 (1)	0.18 (0.048 ... 0.42)	15 (7.8 ... 23)	0.11 (0.045 ... 0.19)	10 (8.4 ... 12)
AFR-44_CSIRO-Mk3-6-0_r1_RCA4 (1)	2.3 (0.32 ... 27)	-6.0 (-20 ... 9.9)	0.50 (0.24 ... 1.0)	4.9 (-0.080 ... 8.9)
AFR-44_EC-EARTH_r12_REMO2009 (1)	0.49 (0.074 ... 2.6)	5.8 (-7.0 ... 21)	0.66 (0.36 ... 1.0)	3.0 (-0.31 ... 6.3)
AFR-44_MPI-ESM-LR_r1_RCA4 (1)	0.31 (0.065 ... 0.87)	11 (1.2 ... 21)	0.84 (0.48 ... 1.2)	1.6 (-2.0 ... 5.4)
AFR-44_MPI-ESM-LR_r1_REMO2009 (1)	0.67 (0.16 ... 2.0)	3.9 (-7.0 ... 16)	0.93 (0.56 ... 1.3)	0.72 (-3.5 ... 5.0)
EC-Earth3P-HR ()	48 (4.5 ... 2.4e+3)	-22 (-33 ... -10)	<not computed>	<not computed>
EC-Earth3P ()	24 (3.1 ... 6.6e+2)	-17 (-28 ... -6.7)	<not computed>	<not computed>

Table 6: *Probability ratio and change in intensity in the* ***24-month SPEI*** *for models that passed the validation tests.*

Model / Observations	a. Past vs. present		b. Present vs. future	
	Probability ratio PR [-]	**Change in intensity ΔI [-]**	**Probability ratio PR [-]**	**Change in intensity ΔI [-]**
CPC	5.5e+3 (33 ... 4.1e+8)	-2.9 (-4.7 ... -1.2)		
AFR-22_CanESM2_r1_CanRCM4 (1)	16 (5.2 ... 76)	-1.4 (-2.0 ... -0.86)	4.1 (3.0 ... 6.8)	-1.1 (-1.2 ... -0.95)
AFR-22_HadGEM2-ES_r1_CCLM5-0-15 (1)	20 (3.5 ... 1.4e+2)	-1.3 (-1.9 ... -0.51)	3.8 (3.1 ... 5.6)	-1.1 (-1.3 ... -1.0)
AFR-22_HadGEM2-ES_r1_REMO2015 (1)	10 (1.3 ... 95)	-1.3 (-2.2 ... -0.13)	3.2 (2.6 ... 4.4)	-1.5 (-1.6 ... -1.3)
AFR-22_MPI-ESM-LR_r1_CCLM5-0-15 (1)	95 (24 ... 7.2e+2)	-2.0 (-2.8 ... -1.2)	3.9 (2.8 ... 6.6)	-1.6 (-1.9 ... -1.3)
AFR-22_MPI-ESM-LR_r1_REMO2015 (1)	2.8e+2 (20 ... 1.4e+4)	-2.5 (-3.3 ... -1.4)	2.5 (2.0 ... 3.5)	-2.7 (-3.1 ... -2.4)
AFR-22_NorESM1-M_r1_CCLM5-0-15 (1)	13 (1.5 ... 1.3e+2)	-1.2 (-2.0 ... -0.19)	3.5 (2.9 ... 4.5)	-1.4 (-1.6 ... -1.2)
AFR-44_CanESM2_r1_RCA4 (1)	12 (3.2 ... 67)	-1.3 (-1.8 ... -0.58)	4.1 (2.9 ... 6.7)	-0.99 (-1.1 ... -0.82)
AFR-44_CSIRO-Mk3-6-0_r1_RCA4 (1)	1.8e+2 (6.4 ... 8.0e+3)	-2.4 (-3.6 ... -0.88)	4.8 (3.9 ... 7.0)	-2.2 (-2.4 ... -2.0)
AFR-44_EC-EARTH_r12_REMO2009 (1)	8.7 (1.4 ... 57)	-1.1 (-2.0 ... -0.16)	2.8 (2.4 ... 3.4)	-1.6 (-1.8 ... -1.4)
AFR-44_EC-EARTH_r3_HIRHAM5 (1)	3.1e+2 (32 ... 1.0e+4)	-2.4 (-3.1 ... -1.5)	7.1 (5.2 ... 12)	-1.6 (-1.8 ... -1.3)
AFR-44_HadGEM2-ES_r1_CCLM4-8-17 (1)	22 (4.4 ... 1.2e+2)	-1.5 (-2.1 ... -0.65)	4.1 (3.3 ... 5.8)	-1.2 (-1.4 ... -1.1)
AFR-44_IPSL-CM5A-LR_r1_REMO2009 (1)	16 (3.9 ... 96)	-1.3 (-1.8 ... -0.62)	3.5 (2.8 ... 4.9)	-1.2 (-1.3 ... -1.1)
AFR-44_MIROC5_r1_RCA4 (1)	9.9 (1.0 ... 75)	-1.4 (-2.5 ... -0.0083)	2.8 (2.4 ... 3.5)	-1.6 (-2.0 ... -1.3)
AFR-44_MPI-ESM-LR_r1_RCA4 (1)	69 (11 ... 1.1e+3)	-1.7 (-2.3 ... -0.96)	3.8 (3.2 ... 5.1)	-1.5 (-1.7 ... -1.4)
AFR-44_MPI-ESM-LR_r1_REMO2009 (1)	3.4e+3 (2.9e+2 ... 2.1e+5)	-2.9 (-3.4 ... -2.2)	8.1 (6.0 ... 13)	-2.0 (-2.1 ... -1.8)
AFR-44_MPI-ESM-MR_r1_RegCM4-3 (1)	45 (3.1 ... 1.9e+3)	-1.9 (-2.9 ... -0.56)	5.1 (3.8 ... 8.2)	-1.7 (-1.9 ... -1.4)
CMCC-CM2-HR4 ()	5.0e+3 (3.4e+2 ... 4.5e+5)	-3.2 (-4.2 ... -2.3)	<not computed>	<not computed>
CMCC-CM2-VHR4 ()	5.2e+2 (31 ... 4.9e+4)	-2.2 (-3.2 ... -1.3)	<not computed>	<not computed>
EC-Earth3P-HR ()	3.1e+6 (2.8e+4 ... 1.2e+10)	-3.4 (-4.1 ... -2.7)	<not computed>	<not computed>

https://doi.org/10.25561/102624

EC-Earth3P ()	5.7e+5 (1.0e+4 ... 1.0e+9)	-3.1 (-3.8 ... -2.4)	<not computed>	<not computed>

Table 7: *Probability ratio and change in intensity in the* ***MAM rainfall*** *for models that passed the validation tests.*

Model / Observations	**a. Past vs. present**		**b. Present vs. future**	
	Probability ratio PR [-]	**Change in intensity ΔI [%]**	**Probability ratio PR [-]**	**Change in intensity ΔI [%]**
CPC	6.9 (0.25 ... 3.6e+3)	-27 (-60 ... 25)		
CHIRPS-CENTrends	1.6 (0.38 ... 7.4)	-8.4 (-30 ... 17)		
AFR-22_CanESM2_r1_CanRCM4 (1)	0.89 (0.30 ... 1.9)	1.7 (-8.9 ... 14)	0.63 (0.41 ... 0.87)	5.3 (1.8 ... 8.8)
AFR-22_MPI-ESM-LR_r1_REMO2015 (1)	2.2 (0.45 ... 10)	-15 (-37 ... 15)	1.3 (0.82 ... 2.1)	-6.2 (-18 ... 4.1)
AFR-22_MPI-ESM-MR_r1_RegCM4-7 (1)	0.58 (0.11 ... 2.4)	15 (-19 ... 62)	1.2 (0.75 ... 1.7)	-3.7 (-16 ... 6.2)
AFR-44_CanESM2_r1_RCA4 (1)	1.1 (0.51 ... 2.3)	-1.9 (-14 ... 14)	0.70 (0.48 ... 0.96)	5.6 (0.74 ... 10)
AFR-44_CNRM-CM5_r1_RCA4 (1)	0.59 (0.18 ... 2.1)	11 (-12 ... 41)	0.87 (0.58 ... 1.3)	2.6 (-4.1 ... 9.3)
AFR-44_CSIRO-Mk3-6-0_r1_RCA4 (1)	5.8 (1.0 ... 1.1e+2)	-25 (-44 ... -0.20)	0.68 (0.40 ... 1.1)	6.2 (-1.1 ... 12)
AFR-44_EC-EARTH_r1_RCA4 (1)	0.70 (0.26 ... 1.9)	6.2 (-9.9 ... 23)	1.0 (0.71 ... 1.4)	-0.71 (-7.1 ... 5.7)
AFR-44_EC-EARTH_r12_RCA4 (1)	1.2 (0.28 ... 6.1)	-3.1 (-25 ... 24)	1.2 (0.76 ... 1.7)	-2.9 (-11 ... 4.5)
AFR-44_EC-EARTH_r12_REMO2009 (1)	0.76 (0.21 ... 2.2)	7.4 (-20 ... 47)	0.89 (0.59 ... 1.2)	2.8 (-5.2 ... 11)
AFR-44_EC-EARTH_r3_RCA4 (1)	3.0 (0.78 ... 12)	-17 (-34 ... 3.6)	1.3 (0.84 ... 1.9)	-4.3 (-11 ... 2.4)
AFR-44_IPSL-CM5A-MR_r1_RCA4 (1)	0.64 (0.18 ... 1.6)	7.3 (-7.9 ... 24)	0.47 (0.26 ... 0.67)	8.7 (5.2 ... 12)
AFR-44_MIROC5_r1_RCA4 (1)	0.22 (0.059 ... 0.55)	32 (11 ... 57)	0.60 (0.33 ... 0.92)	9.0 (1.7 ... 16)
AFR-44_MIROC5_r1_REMO2009 (1)	0.96 (0.30 ... 3.2)	0.89 (-22 ... 34)	1.0 (0.64 ... 1.5)	-1.0 (-11 ... 9.5)
AFR-44_MPI-ESM-LR_r1_RCA4 (1)	0.94 (0.35 ... 2.4)	1.2 (-14 ... 20)	0.87 (0.56 ... 1.2)	2.6 (-3.8 ... 9.5)
AFR-44_MPI-ESM-LR_r1_REMO2009 (1)	2.5 (0.88 ... 9.3)	-18 (-33 ... 3.0)	1.3 (0.84 ... 1.8)	-5.8 (-15 ... 3.8)
AFR-44_MPI-ESM-LR_r2_RCA4 (1)	2.5 (0.80 ... 9.5)	-12 (-25 ... 3.0)	1.2 (0.77 ... 1.7)	-1.9 (-7.2 ... 3.1)
AFR-44_MPI-ESM-LR_r3_RCA4 (1)	2.9 (0.90 ... 11)	-13 (-25 ... 1.2)	1.4 (1.0 ... 2.2)	-5.1 (-11 ... 0.028)

https://doi.org/10.25561/102624

CMCC-CM2-HR4 (1)	20 (3.6 ... 2.1e+2)	-25 (-37 ... -11)	<not computed>	<not computed>
CMCC-CM2-VHR4 (1)	4.6 (0.78 ... 29)	-18 (-35 ... 2.7)	<not computed>	<not computed>
CNRM-CM6-1-HR (1)	31 (4.4 ... 7.7e+2)	-36 (-52 ... -17)	<not computed>	<not computed>
CNRM-CM6-1 (1)	4.6 (1.1 ... 27)	-28 (-51 ... -1.9)	<not computed>	<not computed>
EC-Earth3P-HR (1)	14 (2.2 ... 2.9e+2)	-35 (-54 ... -12)	<not computed>	<not computed>
EC-Earth3P (1)	7.3 (1.2 ... 1.5e+2)	-30 (-51 ... -3.2)	<not computed>	<not computed>
HadGEM3-GC31-HM (1)	6.8 (1.6 ... 58)	-22 (-35 ... -5.7)	<not computed>	<not computed>

Table 8: *Probability ratio and change in intensity in the* ***OND rainfall*** *for models that passed the validation tests.*

Model / Observations	**a. Past vs. present**		**b. Present vs. future**	
	Probability ratio PR [-]	**Change in intensity ΔI [%]**	**Probability ratio PR [-]**	**Change in intensity ΔI [%]**
CPC	0.32 (0.061 ... 2.1)	39 (-17 ... 1.2e+2)		
CHIRPS-CENTrends	0.52 (0.24 ... 1.1)	30 (-4.0 ... 70)		
AFR-22_MPI-ESM-LR_r1_CCLM5-0-15 (1)	0.38 (0.11 ... 0.80)	43 (9.9 ... 82)	0.83 (0.51 ... 1.1)	7.2 (-3.3 ... 18)
AFR-22_MPI-ESM-LR_r1_REMO2015 (1)	0.32 (0.057 ... 0.78)	49 (11 ... 91)	0.81 (0.50 ... 1.1)	7.3 (-4.3 ... 17)
AFR-22_MPI-ESM-MR_r1_RegCM4-7 (1)	0.45 (0.071 ... 1.3)	28 (-9.1 ... 75)	0.41 (0.10 ... 0.83)	20 (9.2 ... 31)
AFR-22_NorESM1-M_r1_CCLM5-0-15 (1)	0.59 (0.14 ... 1.2)	12 (-5.2 ... 35)	0.80 (0.42 ... 1.1)	3.7 (-2.8 ... 10)
AFR-44_CanESM2_r1_RCA4 (1)	0.34 (0.073 ... 0.77)	38 (19 ... 60)	0.37 (0.18 ... 0.62)	16 (13 ... 21)
AFR-44_CSIRO-Mk3-6-0_r1_RCA4 (1)	0.40 (0.099 ... 0.95)	41 (1.7 ... 1.1e+2)	0.69 (0.41 ... 0.98)	9.7 (0.74 ... 19)
AFR-44_EC-EARTH_r12_REMO2009 (1)	0.50 (0.060 ... 1.3)	21 (-8.0 ... 63)	0.75 (0.41 ... 1.0)	6.8 (-0.97 ... 14)
AFR-44_MIROC5_r1_RCA4 (1)	0.63 (0.18 ... 1.5)	11 (-9.7 ... 36)	0.78 (0.50 ... 1.0)	6.6 (-0.69 ... 13)
AFR-44_MPI-ESM-LR_r1_RCA4 (1)	0.52 (0.16 ... 1.1)	17 (-1.8 ... 37)	0.83 (0.51 ... 1.1)	4.1 (-3.9 ... 11)
AFR-44_MPI-ESM-LR_r1_REMO2009 (1)	0.75 (0.28 ... 1.5)	8.8 (-12 ... 34)	0.83 (0.52 ... 1.2)	4.5 (-4.1 ... 13)
EC-Earth3P-HR (1)	0.53 (0.20 ... 1.5)	18 (-8.8 ... 49)	<not computed>	<not computed>
EC-Earth3P (1)	0.99 (0.25 ... 4.7)	0.16 (-24 ... 29)	<not computed>	<not computed>

https://doi.org/10.25561/102624

6 Hazard synthesis

For all the event definitions described above - the MAM rains, OND rains, 24-month rain and 24-month SPEI - we evaluate the influence of anthropogenic climate change by calculating the probability ratio as well as the change in intensity using observations and climate models. Models which do not pass the validation tests described above are excluded from the analysis. The aim is to synthesise results from models that pass the evaluation along with the observations-based products, to give an overarching attribution statement. Figures 6a to 9a show the changes in probability (left-hand side) and intensity (right-hand side) for the observations (blue) and models (red).

In this synthesis, we first add a representation error (in quadrature) to the observations, to account for the difference between observation-based datasets that cannot be explained by natural variability. This is shown in these figures as white boxes around the light blue bars. The dark blue bar shows the average over the observation-based products. Next, a term to account for intermodel spread is added (in quadrature) to the natural variability of the models. This is shown in the figures as white boxes around the light red bars. The dark red bar shows the model average, consisting of a weighted mean using the (uncorrelated) uncertainties due to natural variability. Observation-based products and models are combined into a single result in two ways. Firstly, we neglect common model uncertainties beyond the intermodel spread that is depicted by the model average, and compute the weighted average of models (dark red bar) and observations (dark blue bar): this is indicated by the magenta bar. As, due to common model uncertainties, model uncertainty can be larger than the intermodel spread, secondly, we also show the more conservative estimate of an unweighted, direct average of observations (dark red bar) and models (dark blue bar) contributing 50% each, indicated by the white box around the magenta bar in the synthesis figures.

The model results largely replicate the results in the observations, namely showing an increase in the likelihood and intensity of a 1 in 10 year dry event for the long rains (MAM), a decrease in the likelihood and intensity of a 1 in 5 year dry event for the short rains (OND) and no change for the 1 in 20 year dry event in the 24 months rainfall. While a small number of individual models show different changes, leading to large uncertainties and technically statistically insignificant results, on average the models and observations show very similar changes, quantitatively and qualitatively, rendering the short rain wettening attributable to human induced climate change, while the long rain shows a tendency toward drying. These can be summarised as roughly a doubling in likelihood for the low MAM rains (Fig. 8 (top-left)) with about 11% less rainfall (Fig. 8 (top-right)), although the uncertainty ranges encompass no change. For the short rains (OND) when using the NINO3.4-index as an additional covariate as described above, the likelihood of low rains decreased by about a factor of five (fig. 9 (top-left)) and rainfall intensity increased by approx. 25 % (Fig. 9 (top-right)). The 24-month SPEI, combining the effects of precipitation changes and temperature driven evapotranspiration, shows a very strong increase in the likelihood and intensity of the 1 in 20 year drought event. As is often the case with temperature related indices (van Oldenborgh et al., 2022), the increase in likelihood and intensity in the observations is much larger than in the models, rendering the synthesised results, which show an increase in likelihood of a factor of about 100, conservative (Fig. 7).

These results are corroborated when looking at the same event definitions but instead of in a 1.2C colder climate, in a 0.8C warmer climate (Figs.6b-9b), although the projected changes are much smaller compared with the changes up to now.

Combining lines of evidence from the synthesis results of the past climate, results from future projections and physical knowledge we communicate that the drought severity has increased dramatically because of human-induced climate change. This is primarily driven by the very strong increase in temperature and thus PET, but there is also evidence that this is augmented by drying of the long rains.

https://doi.org/10.25561/102624

(a) Probability Ratio (*left*) and Intensity change (*right*) for current vs. 1.2degC cooler climates

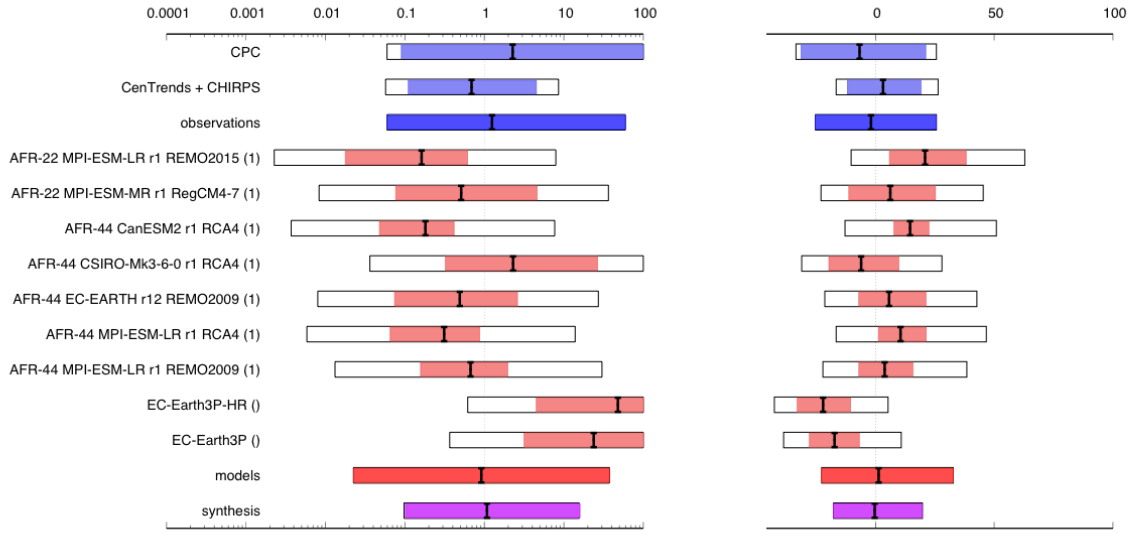

(b) Probability Ratio (*left*) and Intensity change (*right*) for current vs. 0.8degC warmer climates

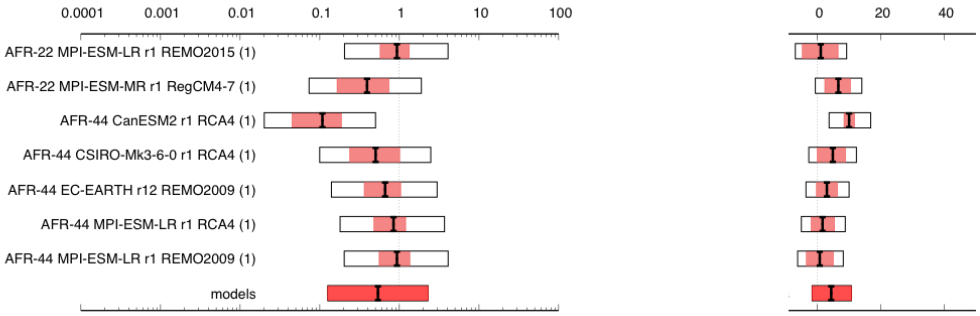

Figure 6: *(a) Synthesis of probability ratios (top left) and intensity changes (in %; top right) when comparing the return period and magnitudes of the 24-month precipitation from 2021-2022 over EA in the current climate and a 1.2ºC cooler climate. (b) same as (a) in the current climate and a future 0.8ºC warmer climate.*

https://doi.org/10.25561/102624

(a) Probability Ratio (*left*) and Intensity change (*right*) for current vs. 1.2degC cooler climates

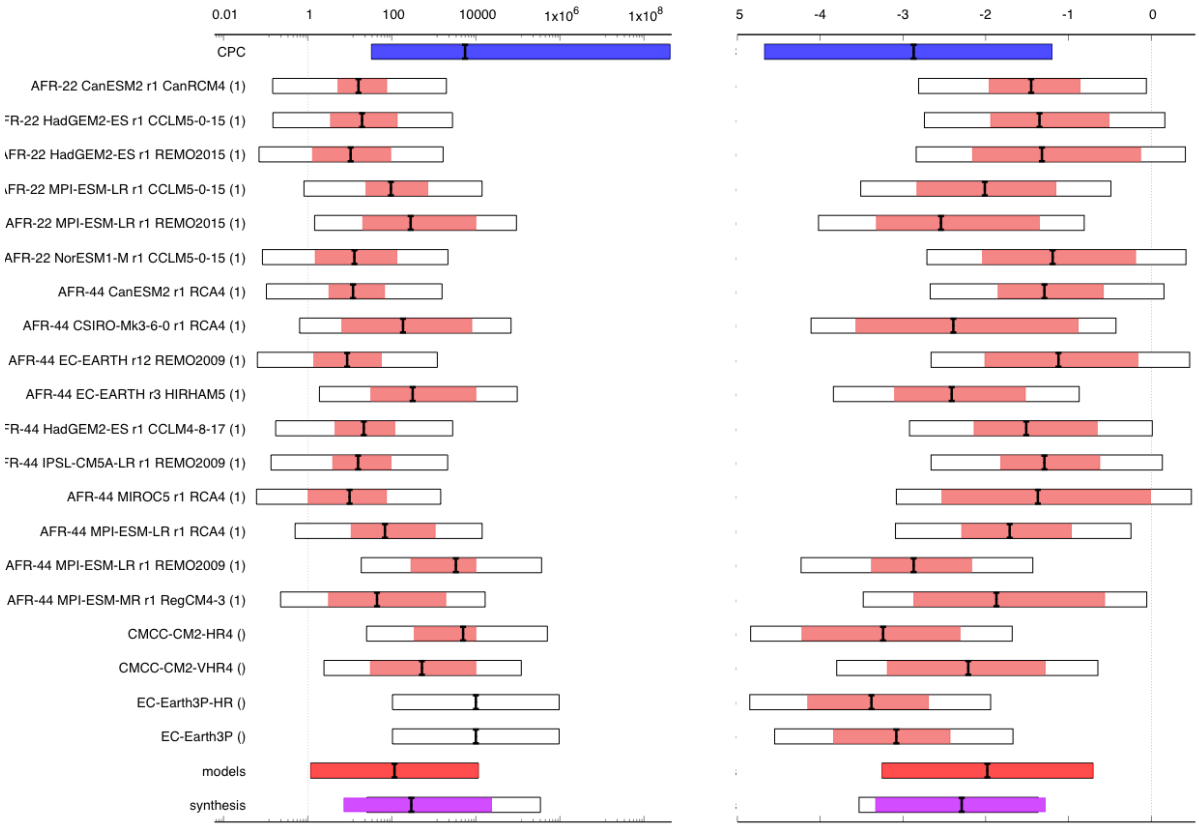

(b) Probability Ratio (*left*) and Intensity change (*right*) for current vs. 0.8degC warmer climates

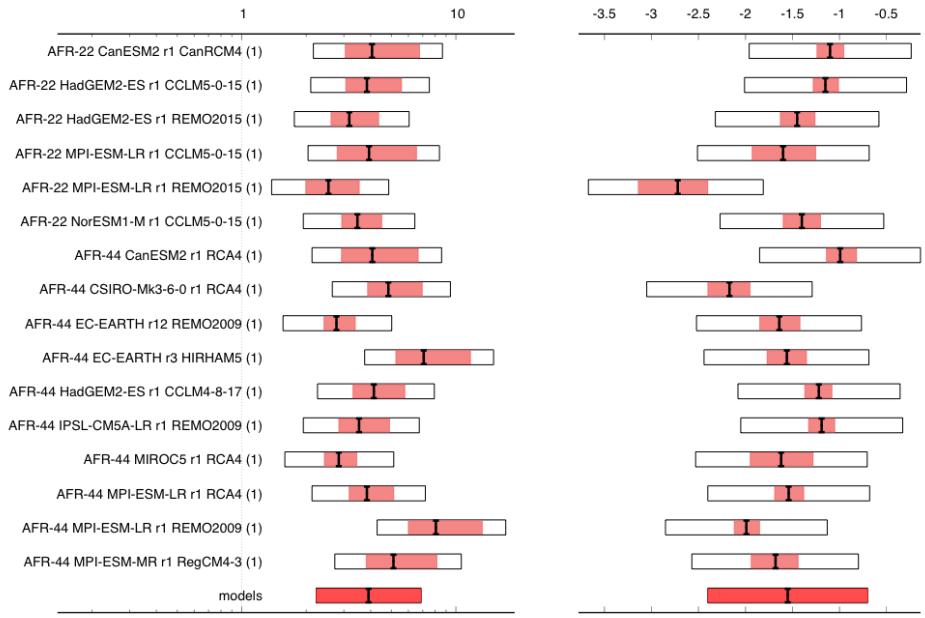

Figure 7: *(a) Synthesis of probability ratios (top left) and intensity changes (in SPEI units; top right) when comparing the return period and magnitudes of the 24-month SPEI over 2021-2022 for EA in the current climate and a 1.2°C cooler climate. (b) same as (a) in the current climate and a future 0.8°C warmer climate.*

https://doi.org/10.25561/102624

(a) Probability Ratio (*left*) and Intensity change (*right*) for current vs. 1.2degC cooler climates

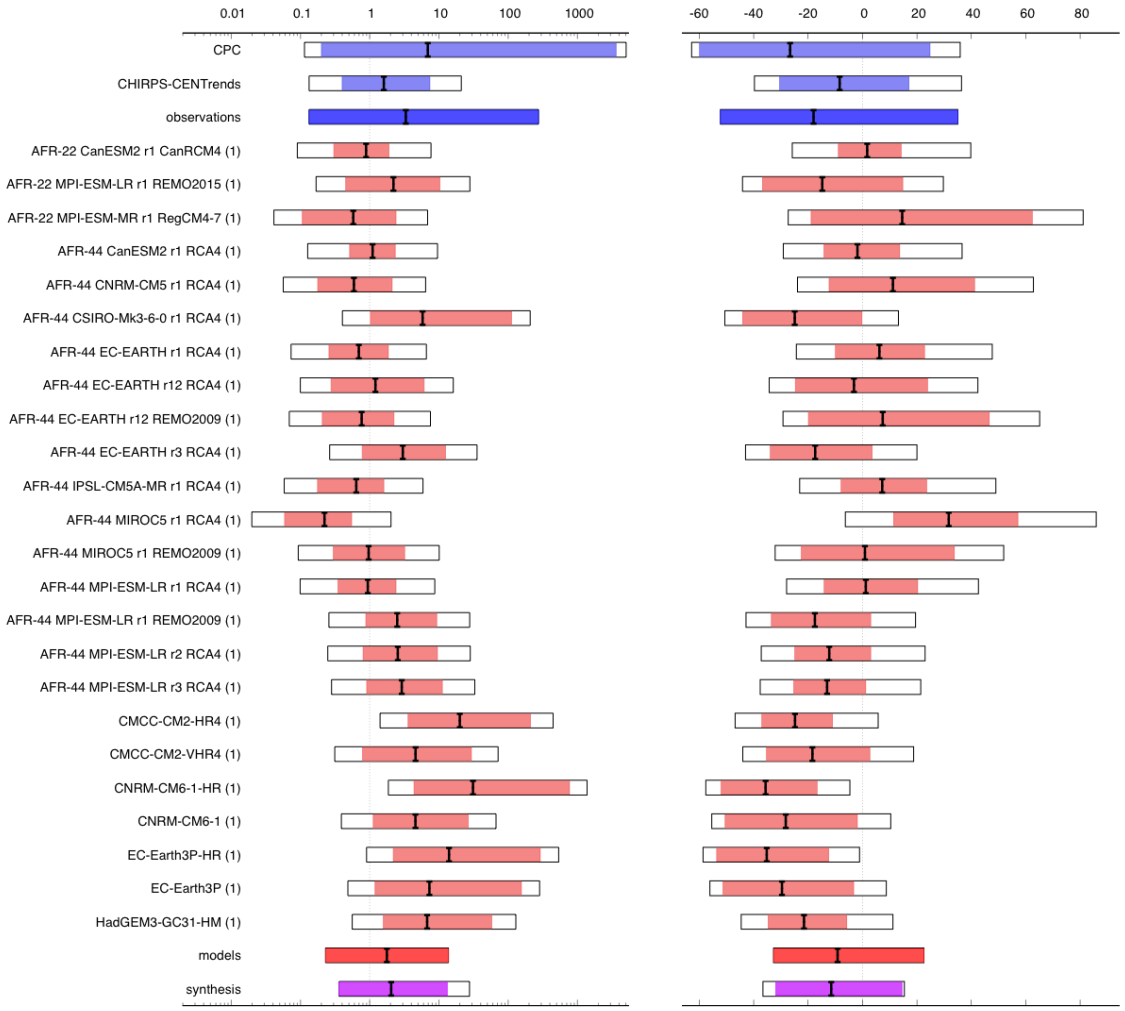

(b) Probability Ratio (*left*) and Intensity change (*right*) for current vs. 0.8degC warmer climates

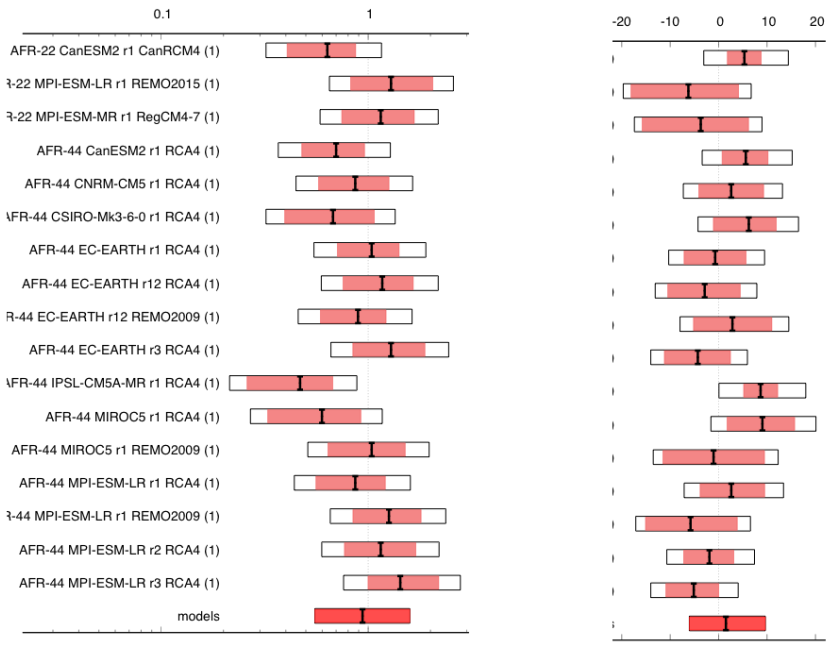

Figure 8: *(a) Synthesis of probability ratios (top left) and intensity changes (in %; top right) when comparing*

https://doi.org/10.25561/102624

the return period and magnitudes of the MAM rainfall over EA in the current climate and a 1.2ºC cooler climate. (b) same as (a) in the current climate and a future 0.8ºC warmer climate.

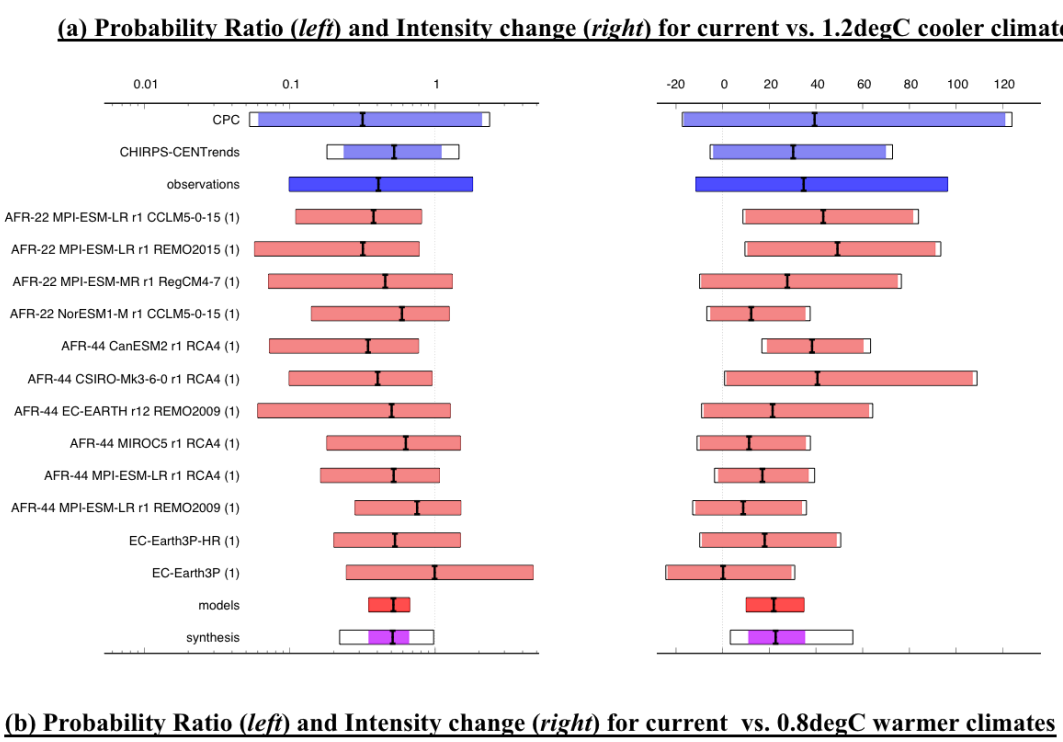

Figure 9: *(a) Synthesis of probability ratios (top left) and intensity changes (in %; top right) when comparing the return period and magnitudes of the OND rainfall over EA using NINO3.4 as an additional covariate in the current climate and a 1.2ºC cooler climate. (b) same as (a) in the current climate and a future 0.8ºC warmer climate.*

7. Vulnerability and Exposure

While changes in hazard are important, climate impacts occur through the confluence of hazard, vulnerability and exposure factors (IPCC AR6). Therefore, it is important to understand the vulnerability and exposure context in which the findings of this attribution study are situated, in order to both acknowledge why the impacts occurred, and to postulate the ways in which to avoid or reduce impacts in the future, as trends of reduced rainfall in the MAM season and high interannual variability continue. This section starts by providing historical context for the current drought and is followed by a look at larger drivers of vulnerability including conflict and fragility, social vulnerability factors,

environmental degradation and land-use changes. This is followed by a look at the drought management and response practices, including national drought management, household coping strategies, early warning and early action, and social protection. Finally, bringing together the vulnerability and exposure factors with the findings of the attribution study we offer some analysis for reducing future drought impacts, and questions for further study.

7.1 Chronic drought exposure

The Horn of Africa (HoA) is no stranger to drought conditions. The disaster database, EM-DAT, records 17-18 drought years for the countries in the study region (Table XX), an underestimate given a lack of records for drought years before 1964 and gaps in data (EM-DAT).

***Table 9**: EM-DAT Drought events 1900 - 2022*

Country	**Drought years**	**# of events**	**# of deaths**	**# of people affected**
Ethiopia	1965, 1969, 1973-78, 1983-84, 1987, 1989-94, 1997, 1998, 1999-2000, 2003-04, 2005-06, 2008-09, 2009-10, 2011-12, 2012, 2015-17, 2021-22	17	402,367	108,041,879
Kenya	1965, 1971, 1979, 1984, 1991-92, 1994-95, 1997-98, 1999-2002, 2004, 2005-06, 2008-09, 2011, 2011-12, 2014-15, 2016-18, 2019, 2020-22	17	196	59,300,000
Somalia	1964, 1969, 1974-76, 1980, 1983, 1987, 1988, 2000-01, 2004, 2005, 2008-09, 2010-11, 2012, 2014-17, 2015-17, 2019, 2021-22	17	39,673	29,019,124

The length of the current drought, five consecutive seasons of below-average rainfall, is unprecedented in the reliable rainfall record which extends back to 1950 (Climate Hazards Centre, 2023). The consecutive nature of the five failed rainy seasons drove higher impacts, as most people may be able to deal with one or two failed seasons, but more than that stretches their resources and tests their ability to cope. For example, warning of possible famine in Somalia after several failed rainy seasons were given and while the official threshold for Famine declaration (IPC Phase 5) has been avoided with increased government and humanitarian aid, there has excess mortality associated with hunger and acute malnutrition occurring concurrently with disease outbreaks (FEWSNET, 2022). Significant interannual variability in rainfall in the region has also created back-to-back cycles of flooding and drought that negatively affects coping capacity (Palmer et al., 2023, Nicolson et al., 2017). In fact, the March to May 2020 season directly before the beginning of this drought was exceptionally wet, leading to floods that killed hundreds of people and displaced hundreds of thousands. The current drought is also driving displacement, which can increase vulnerability, especially of women to gender-based violence, and health risks associated with crowded camps (FEWSNET, 2023). Other compounding factors include the locusts outbreaks (2019-2022) that reduced crop yields, rising global food prices, COVID-19 and the government response all provide a backdrop upon which the drought occurred.

7.2 Conflict and fragility

East Africa has a longstanding history of conflict and fragility directly affected by socio-economic and political drivers and indirectly by climate variability (Owain et al., 2018). Drought and water insecurity have been linked to increased social competition in the region, especially as pastoralists struggle to find pasture for their herds (Meier et al., 2007; von Uexkull et al., 2016). Buhaug et al. (2015) show that socio-economic and political factors have a greater effect on conflict than climatic factors. Despite rapidly growing empirical evidence on the links between climate and conflict (Koubi, 2019; von Uexkull and Buhaug, 2021), analytical challenges remain in the detection and attribution of these links due to the multicausality of conflict and associated impacts (Buhaug et al., 2023). Somalia faces one of the most complex challenges of any country in the world more than 30 years after the state collapsed (Thulstrup et al., 2020). Civil war, the presence of the armed conflict group al-Shabaab hamper serious efforts of statebuilding and peace. Conflict and insecurity continue to intersect with the ongoing drought emergency.

However, conflict and fragility conditions in the presence of weather and climate-related events vary across countries in the HoA region (Thalheimer et al., 2021). In Kenya, the ongoing drought has contributed to an increase in the number of refugee flows that mainly stem from the volatile political and security situations in the neighbouring countries. More than 113,000 Somalis who had arrived in 2022 and in previous years, were officially registered by international organisations to enable them to receive food and other basic assistance. Somalia faces various types of conflict including armed conflict and violence among clans, exacerbating environmental and natural resource challenges (Thalheimer and Webersik, 2020; World Bank, 2020). Recurring extreme wet and dry events across Somalia have also contributed to fragile livelihood outcomes including internal displacement (Thalheimer et al., 2023), see Figure 10. The drought has internally displaced more than 1.4 million people since 2021 and 1.1 million of whom were displaced over the course of 2022 (UNHCR, 2023). Somali refugees are often living in crowded conditions, without access to safe water and sanitation which increase risk of water-borne illness, and increased risk of sexual and gender-based violence, which together with food insecurity increase vulnerability (UNHCR, 2022). Many people have lost their livelihoods with coping capacities stretched too thin to recover from the drought and conflict (see 'Food' in 2021 and 2022 spiking due to conflict and drought, Figure 10). Others have also crossed the border to seek help in Kenya and Ethiopia, joining a large existing refugee population (UNHCR, 2023b). The situation is further compounded by persistent insecurity and armed conflict, soaring food prices, and extreme poverty. These compound vulnerabilities have exacerbated protection risks and pre-existing inequities (Thalheimer et al., 2021b). Notably, women and children make up over 80 percent of Somalia's drought-displaced population, leaving an already vulnerable population even more vulnerable (UNHCR, 2023b; Mason et al., 2007).

https://doi.org/10.25561/102624

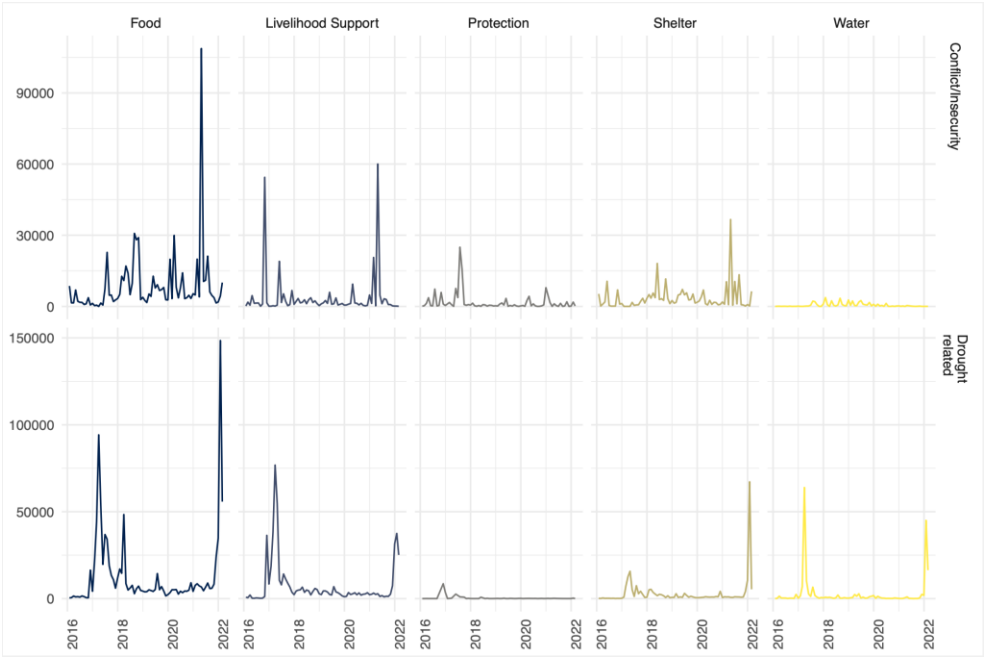

Figure 10: *Priority needs of drought and conflict-affected IDPs in Somalia from Jan 2016 to Dec 2022. Data: UNHCR, 2023.*

7.3 Social vulnerability

For impacts to materialise, a hazard must meet vulnerability (Raju, Boyd and Otto, 2022). To discern what makes people vulnerable, and hit differently, it is essential to examine the prevalence of social vulnerability dimensions, understood as factors influencing individuals' susceptibility to be impacted by a shock (Raduszynski and Numada, 2023). These issues are also pertinent in light of increasing discussions on loss and damage in the context of climate change justice (Boyd et al, 2021; Martin et al, 2022).

Economically and politically marginalised, pastoralists tend to be pushed into working in underdeveloped areas with barren lands, rendering them disadvantaged at the outset (Ayal *et al.*, 2022). When rains later fail and people engaged in weather-dependent livelihoods are forced to spend their limited assets on buffering losses and damages, people are consequently pushed further into poverty, generating a poverty trap (Sherwood, 2013). While this is true for absent and excess rains alike, research suggests that drought is the natural hazard most intimately associated with poverty (Shepherd *et al.*, 2013). In Somalia, drought is known to exacerbate poverty by up to nine percentage points (Pape and Wollburg, 2019). Comparably, in Kenya, climate change adaptation has been shown to reduce poverty when measures adequately confront underlying vulnerabilities, including addressing inequities and improving access to education and health services (Eriksen and O'Brien, 2007). Looking at indicators pertaining to land use, economy, health, energy and infrastructure, social, and water resources, Kenya indicates a decreasing drought vulnerability since 2010, while Somalia and Ethiopia are among the top five most drought vulnerable countries in the world (Ahmadalipour and Moradkhani, 2018; Naumann et al., 2014).

The HoA region is home to a considerable number of people facing chronic food and water insecurity, malnutrition, and limited access to basic services including infrastructure, health care, education, and social protection systems (Prieto-Garcia *et al.*, 2022; OHCHR, 2020; UNDP, 2022). Roughly half the

population in Somalia and Ethiopia are suffering from limited access to energy (Our World in Data, 2020a; Our World in Data, 2020b). Rural communities across all three countries often lack access to electricity altogether (Getie, 2020; Njiru, 2018). In previous droughts across the region, drought conditions in combination with failure of water systems and infrastructure, and increased costs for water, add to worsening impacts (Thomas *et al.*, 2020).

While socioeconomic deprivation increases peoples' exposure and vulnerability to shocks, it decreases communities' abilities to invest in adaptation and risk reduction measures (Vargas Hill and Porter, 2017). Fundamental to food security, health, and income, households engaged in agriculture, agropastoralism, and pastoralism are notably vulnerable to drought and are among the most severely impacted groups when crop and livestock health decline (Prieto-Garcia *et al.*, 2022; Pape and Wollburg, 2019; Bogale and Erena, 2022). Evidence from droughts in Africa clearly highlight malnutrition, and increase in incidence of risk of diarrheal diseases such as cholera (Asmall *et al.*, 2021). In 2022, a team of researchers from the London School of Hygiene and Tropical Medicine and Imperial College London found that 43.000 excess deaths in Somalia can be attributed to the ongoing drought; half of which were children under the age of five (WHO, 2022). In Kenya, the lack of access to clean water faced by women and girls place them at higher risk for complications at childbirth as well as while menstruating (OCHA, 2023). Poorest in the community, elderly people, notably older women, are another disproportionately vulnerable group to climate extremes in the region (Omolo and Mafongoya, 2019). This is in part driven by patriarchal and gender segregating practices such as the gendered division of labour, limiting women's participation in mainstream economic activities (Lwanga-Ntale and Owino, 2020). Even when performing jobs typically held by male counterparts, and becoming the breadwinner, women's influence over decision-making in the household and community remains restricted (Lwanga-Ntale and Owino, 2020).

7.4 Environmental degradation and land-use changes

Over the past decades, the land across the HoA has undergone significant changes which has fueled vulnerability to climate change and the recurring droughts (Prieto-Garcia *et al.*, 2022; Warsame & Sarkodie, 2022). Environmental degradation, unsustainable land-use practices and harvesting, the overexploitation of grazing land and other pastoral activities, deforestation, urbanisation, as well as ongoing conflict have altered the microclimate in the area, causing changes in precipitation patterns that further exacerbate drought conditions, impacting the terrestrial ecosystem, and increasing vulnerability of local communities (Galaty, 2013; Prieto-Garcia *et al.*, 2022). For example, several indigenous plants have been declining including the Yeheb plant, a small tree endemic to the drylands of Ethiopia and Somalia which contains high nutritional and economic value (Prieto-Garcia *et al.*, 2022). Also the large influx of refugees e.g. into Kenya over the years has increasingly stretched the little resources available, contributing further to environmental degradation (OCHA, 2023).

Land grabbing, which involves the conversion of forests lands and grazing lands into large-scale commercial agriculture, biofuel production, or mining operations, has had severe negative impacts on the environment and livelihoods of communities across Sub-Saharan Africa (Borras *et al.*, 2011). Pastoralists are particularly vulnerable to land grabbing due to insecure land rights and inadequate legislative protection, as well as stereotypical views held by policy-makers that tend to justify attempts to grab land in the name of development and for other, more 'productive' uses, such as promises of conservation, preservation of natural resources, national development, and progress (Galaty, 2013). For example, the construction of the Lamu Port-South Sudan-Ethiopia Transport (LAPSSET) Corridor

project from 2012 onwards, aims to connects Kenya, South Sudan, and Ethiopia through a range of transport infrastructure and enhance economic growth yet has been greatly critiqued for violating land rights as well as impacting the environment (Enns, 2017).

Poor institutional arrangements related to land tenure are seen as the primary reason for insecure land rights (Azadi *et al.*, 2021). This problem is exacerbated by unprecedented acquisition of land by international agro-businesses in Africa (World Bank, 2013). Although foreign investment is not entirely undesirable, it often results in investments being carried out at the expense of landholders who depend on their land for food security. In Ethiopia, a large number of foreign investors are now leasing millions of hectares with licences for commercial farms (Graham *et al.*, 2009; Galaty, 2013). Across the Maasai land, pastoral land loss has been lost often gradually, with smaller amounts of land being taken by wealthier herders or transferred to outsiders who seek title-deeds as collateral for loans or long-term investments (Homewood *et al.*, 2009; Rutten, 1992; Galaty, 2013). The development of hydropower plants is also known to drive land dispossession and ultimately strip communities of their ability to sustain their livelihoods, such as in Ethiopia during the development of the Gibe III dam (Schapper, Unrau and Killoh, 2019). The loss of access to traditional grazing lands and water sources contributes to furthering disaster risk and has had devastating effects on pastoralist communities, who rely on mobility and flexibility to manage their herds during times of drought (Lwanga-Ntale and Owino, 2020). Overall, the importance of smallholder farmers, pastoralists, ranchers, and local communities to effectively use their own land remains greatly undervalued, and are marginalised due to inadequate legislative protection, urbanisation, and private investments promoted by the government (Tura, 2018; Galaty, 2013).

7.5. Drought management and response

The impacts of droughts can be mitigated by policies, coping strategies, early warning early action, and eventually drought response. In this case, drought management policy and coordination in the three countries differs significantly, putting them at different starting points to respond to this event. The event itself was well forecasted and warnings were issued but general slow and limited response has been decried. Household coping strategies and responses vary significantly and have a strong impact on the effects felt.

7.5.1. Drought management policies

There are significant differences between drought management policies in the three countries which are important to note as they will have influenced the impacts of the drought event.

Kenya is the only country of the three in the study region which has a dedicated National Drought Management Authority (NDMA, n.d), mandated for all activities related to drought risk management in the country. The Kenyan NDMA provides drought early warning bulletins, develops drought management policies, offers general planning of programmes, and coordinates between various government institutions (NDMA, 2016). The NDMA has a strategic plan which outlines these various spheres; its most recent one ended in 2022 and a new plan 2023-2027 is under revision (NDMA, n.d). Through this, the Kenyan government has taken an integrated approach to drought risk management in which collaboration between the NDMA and various relevant government agencies are key.

In Somalia, the fragmented nature of drought management reflects a situation of chronic humanitarian needs and limited resources, reduced institutional presence and capacity in certain areas. A national drought plan was passed by the government in 2020 with the aim to be a system and mechanism for drought mitigation (Grantham Institute, 2020). The plan was complemented by a drought "Impact & Needs Assessment" run in 2020 which notably studied cross-sectoral drought impacts and needs, and in turn informed the country's "Recovery and Resilience Framework" which sets pathways for resilience building at various levels, including livelihoods (UNDP, 2020). Both Kenya and Somalia are covered by the African Risk Capacity, a disaster risk insurance mechanism of the African Union that allows humanitarian organisations to match funds with existing insurance policies - for instance, in early 2023, Somalia received a payout of USD3.38 million from this fund (Start Network, 2023).
At the community level, both Kenya and Ethiopia implement, Integrated Risk Management programmes within the framework of WFP Ethiopia's Country Strategic Plan (CSP) 2020-2025, as part of the provision of nutrition sensitive social protection, climate risk management services and capacity-strengthening support for smallholder farmers, pastoralists, refugees and returnees most vulnerable to climate shocks (*R4 Rural Resilience Initiative in Ethiopia and Kenya and the Satellite Index Insurance for Pastoralists in Ethiopia (SIIPE) in Ethiopia. WFP, Climate Risk Insurance annual Report 2021*).

Ethiopia's significant devolution of power to the regional level is also a feature of drought risk management in the country – for instance, each region has its own disaster response fund but can apply directly to the federal level for additional funds (Oxfam and Save the Children, 2022). In Ethiopia, lessons from the 2011 drought response led to the launch of a "Disaster Management and Food Security Agency" in 2013 (UNDRR, 2013). Limited information about this system and its relation to drought management can be readily found but seemingly the mandates, status, and activities of this commission have varied significantly over the years.

Generally, there is limited academic research about the achievements and challenges of all these policies and insurance schemes, and will certainly warrant deeper investigation given the humanitarian situation that has arisen. Notably, questions about the applicability of current systems to multiple, consecutive failed rainy seasons, effectiveness of policies in alleviating impacts to food security and human health. It's also important to look at whether the government policies and humanitarian and development interventions have avoided potential impacts and to what extent these systems are contributing to longer-term resilience or reliance.

7.5.2 Household coping strategies

Exposed to recurring weather and climate extremes, rural households have developed different coping strategies to overcome the shocks. While coping strategies may belong to one or more categories, Quandt (2021) offers four distinct classifications. Diversification of livelihood strategies can consist of activities such as salaried employment in other sectors and may involve rural-urban migration or seasonal migration for work (Prieto-Garcia *et al.*, 2022; Taye *et al.*, 2019). Long-term changes to livelihood strategies are conscious efforts to adapt to the hazard, including switching crops, implementing irrigation schemes, and herd management and diversification (Levine et al., 2021; Ayal et al., 2022). These two classifications of coping strategies can largely be labelled non-erosive, and rather constructive, as they help households endure and adapt to drought by finding viable alternatives to current socio-economic practices. Studies show that the most common coping activities among pastoralists in Ethiopia are mobility (82.7 percent) and herd diversification (72.7 percent), with nearly half also engaging in livelihood diversification (Lelamo, Shenkut and Abdilahi, 2022). However, without securing a new livelihood in their new location, migrating in search of meeting their basic needs

often renders people dependent on humanitarian assistance, an erosive coping strategy, which is the case for most displaced persons in Somalia (ACAPS, 2022).

The remaining two coping strategies are considered maladaptive. Erosive measures entail strategies which bring adverse impact on humans or the environment, exacerbate risks, or are unsustainable in the long run (Ahmed, Chowdhury, and Mohona, 2017). Examples of erosive activities notably include producing, burning and selling charcoal; selling or slaughtering livestock; children dropping out of school to support the household; and relying on food assistance (Thulstrup *et al.*, 2020; Taye *et al.*, 2019; Quandt, 2021; Lwanga-Ntale and Owino, 2020). The latter coping activity is common among agropastoralists in Somalia (ACAPS, 2022). In Ethiopia, livestock off-take is practised by almost three out of four pastoralists, whereas one-third engage in charcoal selling (Lelamo, Shenkut and Abdilahi, 2022). When multiple consecutive rainy seasons fail and households find that crisis is the new normal, many short-term coping activities arguably soon also become erosive. These include relying on wild foods and engaging in casual labour (Quandt, 2021).

Risk perception is fundamental to engaging in coping activities (Quandt, 2021). While experiences differ between pastoralists and agropastoralists, research shows that most affected populations' perceive droughts to now occur more frequently, as rainfall is becoming increasingly unpredictable with noticeable changes to the timing and duration of rainy seasons, and temperatures are becoming hotter (Bogale and Erena, 2022; Abrham and Mekuyie, 2022; Abdullah and Mohamed, 2022; Habte *et al.*, 2022). Drying signals for the MAM long rains are indeed clear in the climate models of this attribution study. While the majority of people engaged in weather-dependent livelihoods are also able to predict drought onsets (Bogale and Erena, 2022), the erratic weather, and prolonged, evolving, and compounding state of crisis in the region can be challenging to find adequate coping strategies for, especially for marginalised groups with limited agency. Barriers to undertaking coping strategies abound and include limited finances, expertise, risk information, government support, access to irrigation; shortage of land, labour and finance; as well as conflict (Debela et al., 2019). The ability to translate one's risk perception into non-erosive action moreover depends on the economic, social, and cultural capital households can leverage. Beyond drought risk knowledge and information, undertaking coping activities notably require financial viability and social connectedness (Ndiritu, 2021; Abdullah and Mohamed, 2022; Quandt, 2021; Lwanga-Ntale and Owino, 2020).

7.5.3 Early warning, early action, and response

In 1989, as a reaction to the severe droughts seen in the region in the 1980, the World Meteorological Organization established a centre in Nairobi with the aim to contribute to early warning systems and mitigation of adverse impacts of extreme climatic events on agricultural production (Ambenje, 2004). This centre, renamed and rehoused as the IGAD Climate Prediction and Applications Centre (ICPAC), currently plays a central role in providing the region with weather and climate advisories. Each country in the region also has its own national hydrometeorological agencies which are independent from ICPAC but make significant use of its products and coordination. Notably, the Kenya Meteorological Department (KMD) and Ethiopian National Meteorological Agency (NMA) have two of the largest national forecasting capacities of the Great HoA region.

The seasonal rainfall reflecting the current drought was well forecasted and monitored (e.g. see ICPAC seasonal forecasts and FEWSnet East Africa bulletins). Each of the consecutive failed seasons were accurately forecasted to be below average rainfall by ICPAC and the situation tracked closely by organisations such as the Famine Early Warning System (FEWSnet) and national agencies. Alarm bells

were sounded at least as early as October 2020 with La Nina projections and dry conditions forecasted for the region's rainy seasons:

> *"How firm is the drought prediction? Very. Almost all forecast models and climate agencies anticipate low- er-than-normal rainfall between October and December. My group puts the chance at about 80%. Poor rains in March to May 2021 also seem likely. Of course, there's uncertainty. But that shouldn't prevent action. Forewarned is forearmed." (Funk, 2020)*

Experts warned against a slow response to the drought forecasts (see notably Funk, 2020, Anyadike, 2022). In September 2021, the government of Kenya declared drought as a national disaster (ADRA, 2021); Somalia followed suit in November (OCHA, 2021). A multi-agency drought alert was sounded in December 2021 (FEWSnet. 2021), with a strong call for a humanitarian response.

National drought response generally happens at multiple levels. Theoretically, national governments and their devolved levels of jurisdiction organise the response led by different sectors and agencies; in situations where national capacity is overwhelmed, humanitarian response mechanisms are meant to fill the gaps. In reality, these lines can be less clear, particularly in situations where there is already a significant humanitarian and development presence like in the HoA. Drought response plans in the three countries, coordinated by UN OCHA show significant underfunding compared to the needs estimated by the humanitarian sector (Anyadike, 2022), between 15 and 20% for the three countries (OCHA, n.d).

Table 10: *Status of Drought/Humanitarian Response plans funding (OCHA, financial tracking service)*

Country	**Kenya**	**Ethiopia**	**Somalia**
Funded action	USD 65.9 million	USD 781.6 million	USD 582.8 million
Requirements	USD 451.8 million	USD 3994.8 million	USD 2599.2 million
Summary of action clusters	Education, Food security and livelihoods, Health, Nutrition, Protection, Water, sanitation, and hygiene	Camp Coordination and Camp Management, Education, Food security and livelihoods, Health, Logistics, Nutrition, Protection, Refugee Response, Shelter and NFIs, Water, sanitation, and hygiene	Agriculture, Camp Coordination and Camp Management, Education, Food, Health, Logistics, Nutrition, Protection, Shelter and NFIs, Water, sanitation, and hygiene

Other initiatives have also been taken by the countries to respond to the drought over the last few years. For example in Kenya, a flash drought appeal launched by the government and humanitarian organisations supported 1.7 million people between October 2021 and late 2022, and the Kenyan Red Cross activated an early action protocol in October 2022 to support at-risk farmers (IFRC, 2022).

https://doi.org/10.25561/102624

Questions about the effectiveness and reach of various types of warnings and the design of drought response including the humanitarian aid paradigm and many more should be unpacked and investigated in subsequent analysis.

7.5.4 Social protection

Kenya and Ethiopia both have strong social protection systems which are often regarded as flagship examples for the broader region. In Kenya, this includes the Hunger Safety Net Programme (HSNP) which was launched in 2007 and is run by the National Drought Management Authority (NDMA). The HSNP is one of four cash transfer based social protection systems in Kenya under the National Safety Net Programme (PSNP). The other three systems include: the Older Persons Cash Transfer (OPCT) programme, Cash Transfers for Orphans and Vulnerable Children (OVC), and Persons with Severe Disability Cash Transfer (PWSD-CT) programme. The HSNP aims to provide financial security to, and reduce hunger of, the most vulnerable Kenyan's, especially in the Arid and Semi-Arid Lands (ASAL) of Northern Kenya (HSNP, 2023). As of June 2022, the HSNP's reach includes 149,000 households, including scaled-outreach, provided with unconditional cash transfers at a value ranging from 2,700KES (20USD) to 5,400 KES (40USD) on a monthly or bi-bimonthly basis. (NDMA, 2022). Collectively the four safety net programmes reach one million households across Kenya and humanitarian actors, such as WFP are further supplementing with food assistance to approximately 175,000 households as of February 2023 (FEWSNET, 2023).

The HSNP includes a trigger based model for scaling up or down its support to vulnerable households. This model is based on the Vegetation Condition Index with four tiers of potential drought severity, ranging from no drought to extreme drought. In the case of extreme drought, the system is designed to include 75% more vulnerable households in affected areas (HSNP, 2023). An assessment of the HSNP systems operation during its first phase from 2009 to 2012, indicated that 87% of beneficiary households had an increased number and size of meals as a result of the program. The same brief notes that in 2015 the 'HSNP was also able to scale-up assistance within two weeks to 90,648 additional households following severe and extreme drought' (ODI, 2017).

Similarly the Productive Safety Net Programme (PSNP) is a flagship programme launched by the Ethiopian Government in 2005, with its fifth phase launched in 2021 to last until 2026. The PSNP, a complement to additional SP systems in Ethiopia, is a multi-billion dollar program that enhances food and economic security, while building resilience against crises. The PSNP provides cash payments to able-bodied members in exchange for engaging in labour contributions toward public works projects, and it provides direct payment for six months of the year to more vulnerable households. The PSNP is designed to reach up to 9 million people per year (USA, 2021). A 2022 study of the PSNP found that the PSNP enhances daily calorie intake (by 14.5%), consumption expenditures (by 26%), access to credit services (by over 68%) and annual income of participating households (57.7% higher) when compared with a control group (Tadesse and Zeleke, 2022). Relative to non-beneficiaries, PSNP recipients experienced 57 percent lower impacts of drought on food security (Scognamillo, Mastrorillo and Ignaciuk, 2022). Notably, recipients were able to absorb drought shocks more quickly (less than two years), and 48% less likely to face crop failure (Scognamillo, Mastrorillo and Ignaciuk, 2022). A similar study by Abay et al. (2022) also found that the PSNP produced positive resilience outcomes at a household level, especially for households receiving transfers above the median transfer level, and those in the program for longer durations. At the same time, the ongoing conflict in Ethiopia's Tigray, Amhara and Afar regions has impacted the PSNPs timelines and reach (New Humanitarian, 2022; World Bank, 2021).

https://doi.org/10.25561/102624

In Somalia, social safety net programs are predominantly delivered via NGOs and local administrators with support from international partners. Approaches include both conditional and unconditional cash transfer programs as well public work programmes and school feeding programs. According to a study by Florence et al. (2021), "*the inherent challenges in these programmes included inadequate funding, low coverage, short-term implementation periods, and inadequate involvement of the Federal Government of Somalia (FGS) and Federal Member States (FMS) actors.*" In 2019, the Government of Somalia' Ministry of Labor and Social Affairs, World Food Programme, UNICEF and the World Bank jointly launched the Shock-Responsive Safety Net for Human Capital Project (SNHCP), known as *Baxnaano.* The goal of this programme is to enhance food security and increase economic resilience. In 2020 the programme reached 1.2 million people across Somalia, with capacity to scale-up to additional households in response to shocks. The Baxaano project incorporates a short and long-term perspective including nutrition-lined unconditional cash transfers (20USD per month), enhancing social safety net delivery systems and institutional capacity building (WFP, 2021; World Bank, 2022).

Based on historical events, the HSNP and the PSNP are critical components in mitigating what could be worse impacts of the ongoing drought. At the same time the drought severity and extent requires support beyond these systems. This signals a need to further scale the systems geographic extent (especially in Kenya), while also underscoring the need for SP and humanitarian systems to work hand-in-hand during emergencies.

In addition to the formal social protection system, there is an extensive informal social protection system amongst people in East Africa which includes remittance flows from abroad. Informal social protection takes forms that are based on ties of social solidarity deriving from shared kinship, religion, locality or friendship. These examples of social capital bind individuals and groups together, promoting a pooling of risks and shared responses to livelihood risks. Such mechanisms are themselves, however, vulnerable to shocks and stresses. External assistance can build on and help to strengthen the linking social capital functions of such informal mechanisms, enabling them to contribute more effectively to 'shock-responsive' social protection. These should be seen as complementary to, formal social protection, which remains the responsibility of the state.

In cases where the provision of social assistance (through government or humanitarian system) is unavailable or inaccessible, collective modalities of support outside a rights-based framework take on greater significance. These forms of provision are described as being informal as opposed to the formality of provision offered through state actors or the international humanitarian system. This neat binary of formal/informal occludes the embedded character of the informal in the everyday lives of those receiving social assistance (Zaman et al., 2022).

In Ethiopia for example, Sabates-Wheeler et al. (2013) identify features within pastoral groups and recognise that network-based distribution provides important functions in mitigating the consequences of livelihood crises and that local authority structures provide functions on social and economic issues beyond the interface with external assistance (Sabates-Wheeler et al., 2013).

7.6 V&E conclusions

The impacts of this drought are far-reaching, touching on aspects such as health, food security, livelihoods, displacement, electricity infrastructure, security, and governance. The impacts differ by country based on vulnerability and exposure factors that determine severity, with Somalia's fragility

particularly limiting people's ability to meet basic needs, driving displacement and increased mortality (FEWSNET, 2022). Factors like disaster management and response functions, international aid, livelihood type, socio-economic status, state fragility, and the length of the drought play a role in determining where and for whom impacts are greatest.

Given the drying trend in the MAM season, there are implications for short-term drought management and long-term adaptation. The severe impacts of this drought could be interpreted as a shortcoming of current drought management systems, or it could be attributed to the severity and length of the drought, or, most likely, a combination of the two.

How many failed rainy seasons should government drought management systems and the international aid infrastructure be prepared to handle? Generally, limits to adaptation are divided into soft limits, those that could be overcome with technological and socioeconomic support which are plausible but not currently available, whilst hard limits are reached when there are no longer any feasible adaptation options (IPCC, AR5; Dow *et al.*. 2013; Mechler *et al.*, 2020).

Notably, drying signals for the MAM long rains are clear in the climate models (section 6) and therefore people and communities need to adapt. In turn, the vulnerability and exposure dynamics explored above provide us with the underlying factors that can amplify or conversely, reduce risks.

While more and better designed social protection systems and humanitarian funding may help decrease poverty and increase resilience to shocks when they occur, certain crops, animals, and by extension livelihoods may become increasingly difficult to sustain in the changing climate. Similarly, continuing conflict and land tenure law are posing significant barriers to adaptation possibilities but these situations may change.

A focus on reduction of vulnerability and exposure, approaches that are robust to both wet and dry extremes, and increasing the capacity of people to cope with these types of events could support short-term and long-term adaptation and resilience. Having a holistic understanding of vulnerability can help reduce maladaptation that comes from reinforcing existing inequities (Eriksin *et al.*, 2021).

Data availability

Almost all data are available via the KNMI Climate Explorer. Python notebooks used in the preparation and analysis of the observation and model data are available via GitHub.

https://doi.org/10.25561/102624

Appendix

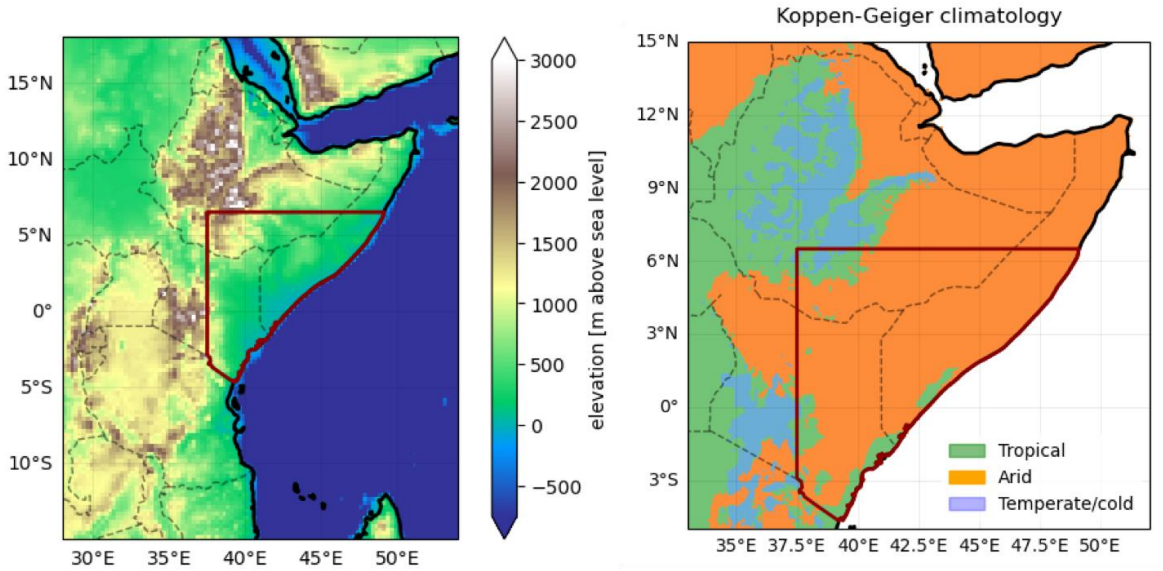

***Figure A1: Left**: Elevation map, produced using [TBASE data] at 0.25° resolution. **Right**: Koppen-Geiger climate classification map, using data from [GloH2O].*

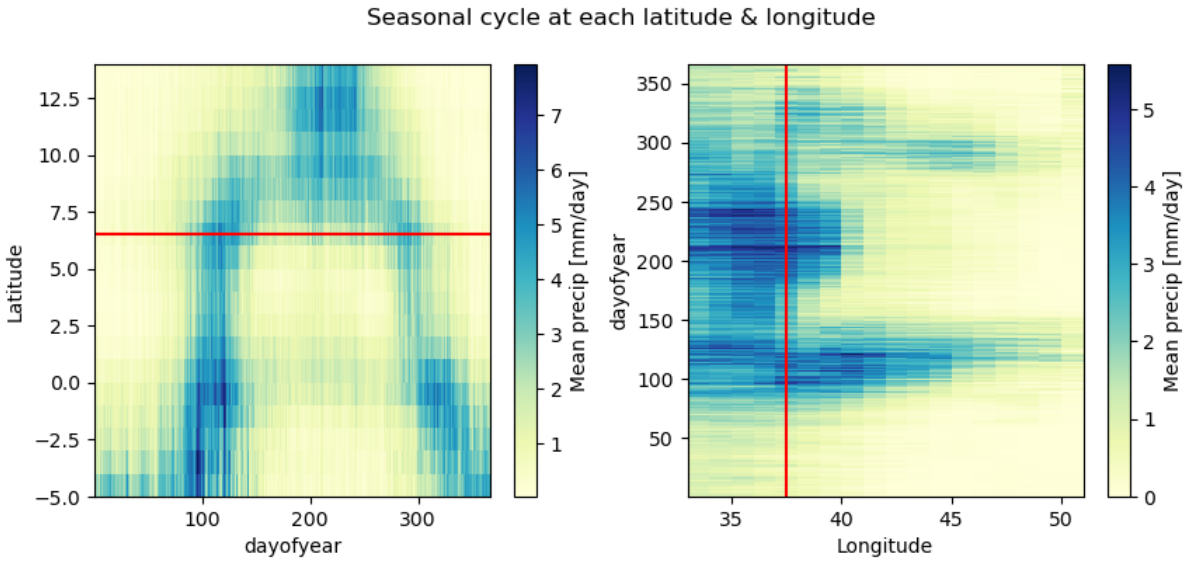

***Figure A2:** The variation in seasonal cycle of precipitation across latitudes (left) and longitudes (right), for EA. The red line through the latitude (or longitude) separates the part of the region with distinct long and short rain seasons, from the part with rainfall in JJAS.*

https://doi.org/10.25561/102624

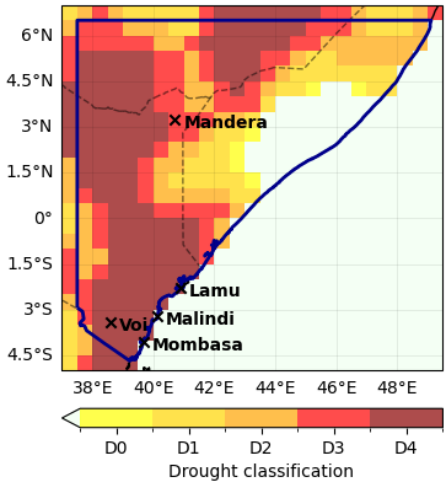

Figure A3: *Locations of five stations used to validate the gridded observational datasets. Recent station data are not available for much of the study region, including all of Somalia and Ethiopia.*

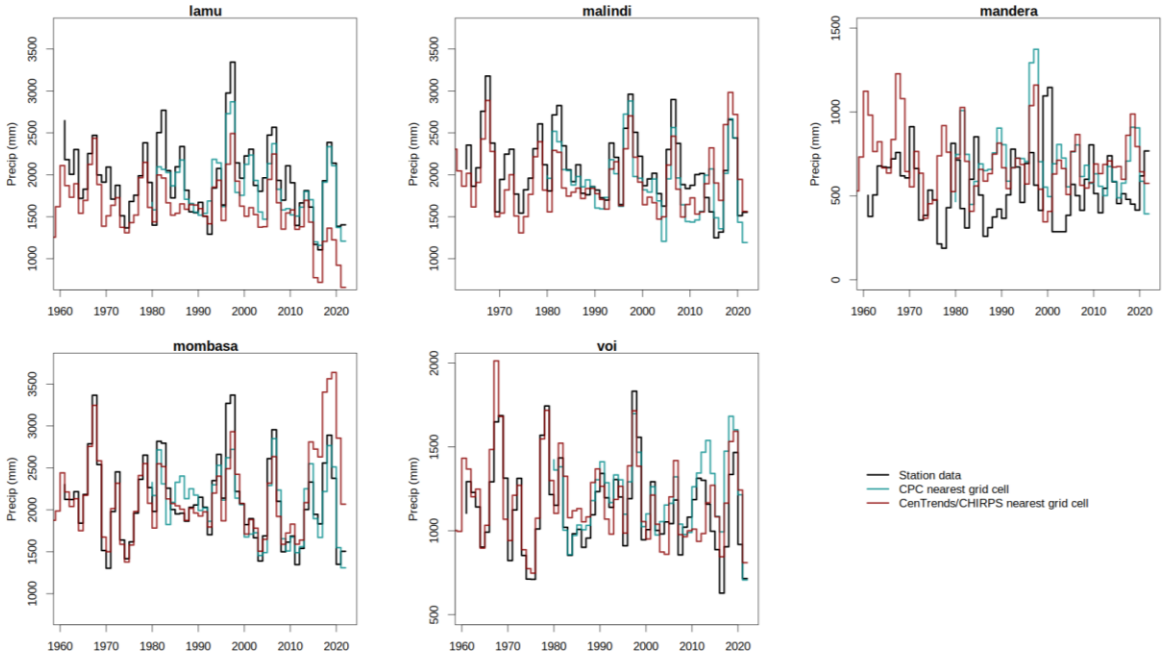

Figure A4: *validation of gridded datasets using station data. In all cases, the CPC time series more closely follows the station time series, supporting the choice of this dataset as the primary basis for analysis.*

https://doi.org/10.25561/102624

Table A1: *Fitted coefficients from linear models of base 10 logarithm of precipitation (log10precip) with GMST only (Model 1) as covariate and both GMST and Nino as covariates (Model 2) for the short rains. Significant coefficients at 5% level are marked with * and highlighted in bold.*

Model 1: log pr~GMST; ***Model 2***: log pr~GMST+Nino		
Dataset	**Model 1: GMST only**	**Model 2: GMST & Nino**
CPC	0.1704	0.3253 & **0.1878***
CenTrends-CHIRPS	0.2439	**0.3107*** & **0.189***

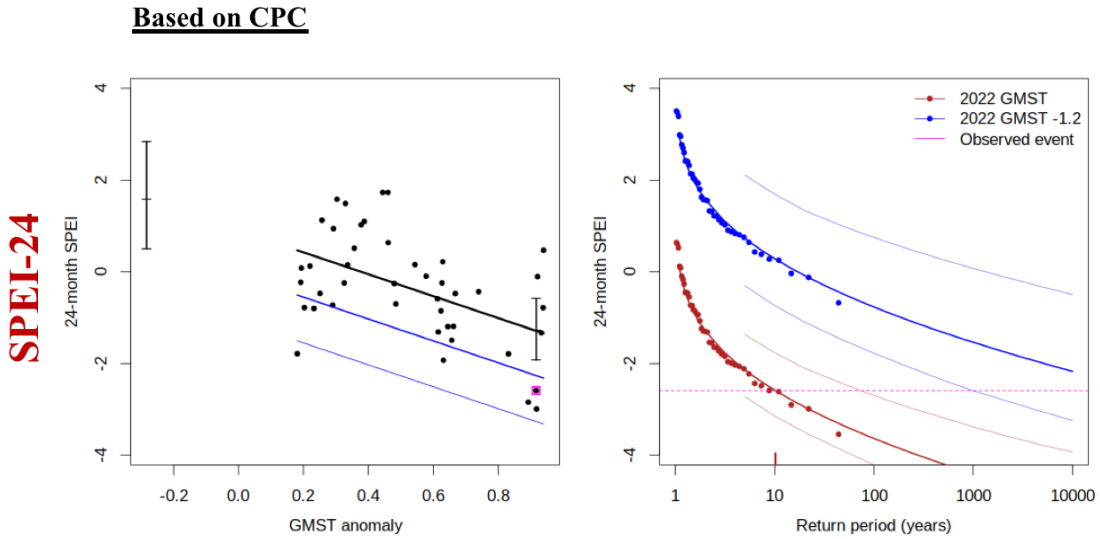

Figure A5. Left: *Response of SPEI-24, computed from CPC mean 24-month precipitation and mean 24-month PET over the study region, to change in global mean temperature. The thick black line denotes the time-varying mean, and the blue lines show 6- and 40-year return levels. The vertical black lines show the 95% confidence interval for the location parameter, for the current climate and a hypothetical 1.2ºC cooler climate. The 2022 observation is highlighted with the magenta box.* ***Right:*** *Gaussian-based return periods of log-transformed rainfall for the 2022 climate (red lines) and a 1.2ºC cooler climate (blue lines) with 95% CI, based on CPC dataset.*

https://doi.org/10.25561/102624

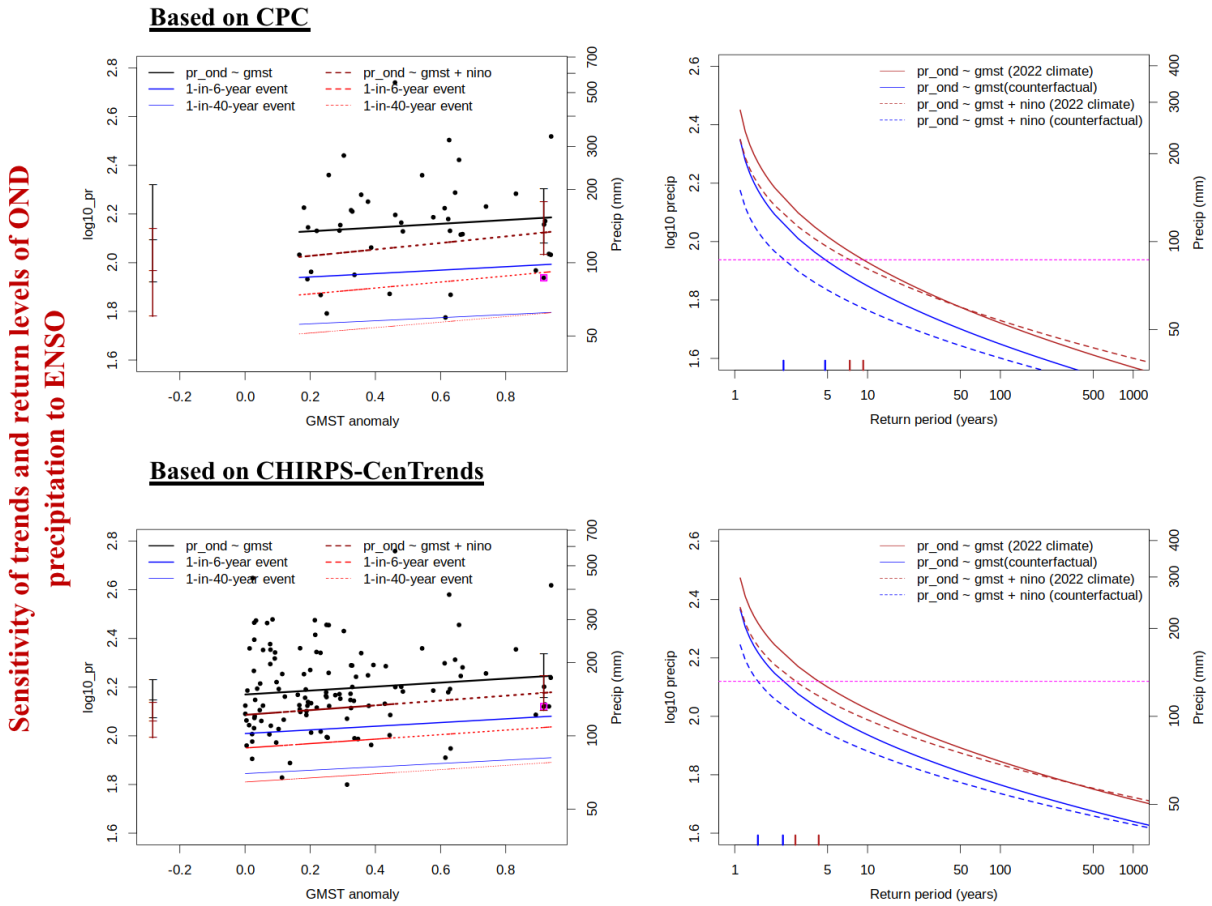

Figure A6: ***Top:*** *Comparison between the GMST response of OND rainfall when conditioned on 2022 value of Nino3.4 vs. without conditioning on Nino3.2 from CPC (left) and CenTrend-CHIRPS datasets (right) ,* ***Right (top):*** *Gaussian-based return periods of log-transformed rainfall for the 2022 climate (red lines) and the 1.2ºC cooler climate (blue lines with 95% CI), for the same two cases, based on CPC (left) and CenTrend-CHIRPS datasets (right).*

Acknowledgements

Emmanuel Raju, *Department of Public Health, Global Health Section & Copenhagen Centre for Disaster Research, University of Copenhagen, Denmark.*
Shaban Mwanda, *Red Cross Red Crescent Climate Centre, The Hague, the Netherlands.*
Phoebe Wafubwa Shikuku, *International Federation of Red Cross and Red Crescent Societies (IFRC), Geneva, Switzerland.*

Please cite this paper as:
Kimutai, J; Barnes, C; Zachariah, M; Philip, S; Kew, S; Pinto, I; Wolski, P; Koren, G; Vecchi, G; Yang, W; Li, S; Vahlberg, M; Singh, R; Heinrich, D; Pereira, CM; Arrighi, J; Thalheimer, L; Kane, C; Otto, FEL (2023). Human-induced climate change increased drought severity in Horn of Africa.
DOI: https://doi.org/10.25561/103482

https://doi.org/10.25561/102624